CHARLES UNIVERSITY

Faculty of Science

Department of Parasitology

Study program: Parasitology

Bc. Ekaterina Panova

Importance of CIA pathway proteins in the formation of Fe-S clusters in the nuclei of *Giardia intestinalis*

Úloha proteinů CIA dráhy při tvorbě Fe-S klastrů v jádrech *Giardia intestinalis*

DIPLOMA THESIS

Supervisor: Mgr. Pavel Doležal, Ph.D.
Consultant: Mgr. Martin Benda, Ph.D.

Prague 2025

Prohlášení:

Prohlašuji, že jsem závěrečnou práci zpracovala samostatně a že jsem uvedla všechny použité informační zdroje a literaturu. Tato práce ani její podstatná část nebyla předložena k získání jiného nebo stejného akademického titulu. Při zpracování této diplomové práce byl využit nástroj umělé inteligence ChatGPT (OpenAI) pro jazykovou korekci textu a vyhledávání odborných článků. Výsledná interpretace a odborný obsah však byly zpracovány samostatně.

V Praze dne 7. 8. 2025 ……...……..

Ekaterina Panova

Acknowledgements:

I would like to thank my supervisor, Mgr. Pavel Doležal, Ph.D., for his time, guidance, and support throughout my bachelor's and master's studies. I'm also grateful to my consultant, Mgr. Martin Benda, Ph.D., for his patient instruction in lab techniques and constant readiness to help. Thanks to all members of our lab and BIOCEV team for their support, advice, and positive environment. Finally, heartfelt thanks to my family and partner for their patience and emotional support during this journey.

Abstract

Iron-sulphur (Fe-S) clusters are essential cofactors for nuclear proteins involved in DNA replication and repair. In eukaryotes, their maturation depends on the iron-sulphur cluster assembly (ISC) and cytosolic iron-sulphur cluster assembly (CIA) pathways. *Giardia intestinalis*, has reduced organelles and minimal system for iron-sulphur clusters biogenesis, is a simplified model to study this process.

The main aims of this work are to identify candidate nuclear Fe-S proteins, analyse their expression and localization, and investigate the function of selected CIA pathway components using CRISPR/Cas9-mediated gene knock-out. Particular attention is given to Nbp35_3, a scaffold protein believed to play a central role in Fe-S cluster assembly.

Key words: *Giardia intestinalis*, Fe-S cluster, CIA pathway, nuclear proteins, Nbp35, knock-out, mitosome.

Abstrakt

Železo-sirné (Fe-S) klastry jsou nezbytné kofaktory pro jaderné proteiny podílející se na replikaci a reparaci DNA. U eukaryot jejich maturace závisí na mitosomalní (ISC) a cytosolické (CIA) dráze syntézy Fe-S klastrů. *Giardia intestinalis* s redukovanými organelami a minimálním systémem pro biogenezi Fe-S klastrů představuje zjednodušený model pro studium těchto procesů.

Hlavním cílem této práce je identifikace kandidátních jaderných Fe-S proteinů, analýza jejich exprese a lokalizace a zkoumání funkce vybraných složek CIA dráhy pomocí genové inaktivace technikou CRISPR/Cas9. Zvláštní pozornost je věnována proteinu Nbp35_3, scaffoldovému proteinu, který pravděpodobně hraje klíčovou roli v sestavování Fe-S klastrů.

Klíčová slova: *Giardia intestinalis*, Fe-S klastr, CIA dráha, jaderné proteiny, Nbp35, knock-out, mitozom.

Contents

1 Introduction

Iron-sulphur (Fe-S) clusters are ancient inorganic cofactors essential for a broad range of cellular processes, including electron transport, redox switching and regulation of genome stability. In eukaryotes, the maturation of Fe-S proteins depends on two compartmentalized biosynthetic systems: the mitochondrial iron-sulphur cluster (ISC) assembly machinery and the cytosolic iron-sulphur cluster assembly (CIA) pathway. The CIA pathway is responsible for the insertion of Fe-S clusters into cytosolic and nuclear apoproteins, which are involved in critical functions such as DNA replication and repair.

Giardia intestinalis is a microaerophilic parasitic protist with a highly reduced cellular structure, possessing mitosomes instead of conventional mitochondria. These organelles have retained only a Fe-S cluster biosynthesis function. Despite this, *G. intestinalis* maintains a minimal functional CIA pathway, making it a great model for studying essential components of Fe-S cluster assembly.

This thesis investigates the role of CIA pathway components in the maturation of nuclear Fe-S proteins in *G. intestinalis*. It focuses on identifying nuclear Fe-S proteins, analysing their expression and localization, and using CRISPR/Cas9 to disrupt CIA proteins. Special attention is given to Nbp35_3, a cytosolic scaffold protein, which plays a central role in Fe-S cluster assembly.

By examining how *G. intestinalis* maintains nuclear Fe-S protein biogenesis with a reduced set of CIA pathway proteins, this work helps to understand the essential machinery required for the process and demonstrates how critical cellular functions can be maintained in a highly adapted anaerobic parasite.

2 Review of literature

2.1. Giardia intestinalis

Giardia intestinalis (synonyms *Giardia lamblia* or *Giardia duodenalis*) is a microaerophilic unicellular protist parasite that infects human and other mammals. It is classified as a diplomonad within the phylum Metamonada (Cavalier-Smith 2003).

G. intestinalis has a life cycle alternating between the cyst and trophozoite stages. Infection begins when cysts are ingested through contaminated water or food. Trophozoites are released in small intestine by excystation and attach to the epithelium. They multiply and cause the disease symptoms by attaching and damaging the epithelium. As *G. intestinalis* moves toward the colon, the resistant cysts form during a process known as encystation. Then the cysts are excreted and remain infectious in the environment (Adam 2021).

Giardiasis is an intestinal disease with global distribution. It is especially common in children from low- and middle-income countries. The global incidence of symptomatic giardiasis is approximately 15 cases per 100 children/year. Key risk factors are poor sanitation, contaminated water and poor hygiene (Gutiérrez et al. 2024).

G. intestinalis lacks several classical eukaryotic organelles, including mitochondria, peroxisomes, and a typical Golgi apparatus (Tovar et al. 2003; Faso and Hehl 2011). Despite this, it contains highly reduced mitochondria-derived organelles known as mitosomes, which are not involved in energy production and remain only one function – Fe–S cluster biosynthesis (Tovar et al. 2003).

2.2 Iron-sulphur clusters

Fe-S clusters are inorganic cofactors of many biological systems. These clusters play a key role in a wide variety of biological processes, including electron transfer, redox catalysis, and gene regulation. Fe-S clusters are also redox sensors, responding to oxidative stress, and regulate the activity of the proteins (Johnson 1998; Tsaousis 2019).

These cofactors are composed of iron and sulphide ions and coordinated by cysteine residues in proteins. Clusters exist in various forms such as rhombic [2Fe-2S], asymmetrical [3Fe-4S], cubane [4Fe-4S] (*Fig.1*), and even larger assemblies like

[8Fe-7S] and [8Fe-9S] (Ohki et al., 2009). They are able to switch between oxidation states, which makes them key components in enzymatic and regulatory pathways involving redox reactions (Johnson 1998).

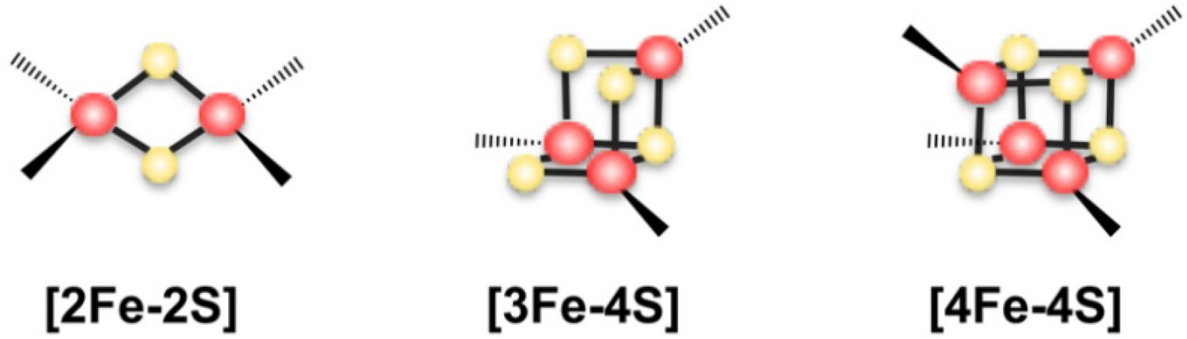

Figure 1: Three common types of Fe-S clusters. From left to right: the rhombic [2Fe-2S] cluster, the asymmetrical [3Fe-4S] cluster, the cubane [4Fe-4S] cluster. Red spheres represent iron ions, while yellow spheres represent sulphur ions (Mendel et al. 2020).

Several cytosolic enzymes containing [4Fe-4S] or [2Fe-2S] clusters play a central role in the metabolism of *G. intestinalis*. These enzymes are essential for anaerobic energy production, redox balance, and stress response. Pyruvate:ferredoxin oxidoreductase (PFOR) is a key cytosolic enzyme in *G. intestinalis* that converts pyruvate to acetyl-CoA and transfers electrons to ferredoxin via [4Fe-4S] clusters. It plays a central role in anaerobic energy metabolism and drug activation (Townson et al. 1996; Emelyanov and Goldberg 2011).

Another cytosolic protein, which contains [2Fe-2S] cluster, is ferredoxin. This enzyme acts as electron carrier in anaerobic metabolism. It receives electrons from PFOR and transfers them to other enzymes such as hydrogenase or nitroreductase (Duwor et al. 2024). Hydrogenase, which contains [4Fe-4S] cluster, then uses this reduced ferredoxin to produce molecular hydrogen (H_2) by transferring electrons to protons. This process regenerates oxidized ferredoxin (Emelyanov and Goldberg 2011).

G. intestinalis also possesses a nitric oxide reductase (NOR), a [4Fe-4S] cluster containing protein, that helps parasite to survive in low-oxygen environments (Crack et al. 2014). This enzyme also detoxifies nitric oxide (NO), which is produced by the immune system of the host, by converting it into nitrous oxide (N_2O) (Rafferty et al. 2010; Di Matteo et al. 2008). These Fe-S proteins are formed via the CIA pathway (Braymer et al. 2021).

2.3 Biogenesis of Fe-S clusters

To begin with, it is important to note that distinct nomenclatures are being used to describe biogenesis pathways in different eukaryotic and prokaryotic species. In this work, the yeast nomenclature will be used.

In eukaryotes, the biogenesis of Fe-S clusters starts in mitochondria or mitochondria-related organelles through the iron-sulphur cluster (ISC) assembly machinery. This process begins in early ISC pathway with activity of the cysteine desulphurase Nfs1, which provides sulphur ions from cysteine, which is then converted to alanine. Nfs1 forms a stable complex with Isd11 and Acp1, ensuring structural stability and catalytic activity. Sulphur ions are subsequently transferred from the Nfs1 to the scaffold protein Isc1/2, where are combined with iron ions. Nfs1 is regulated by frataxin, by modulating the catalytic efficiency of the Acp1-Nfs1-Isd11 complex. This coordinated assembly leads to the formation of a [2Fe-2S] cluster. This can serve as a precursor for forming a [4Fe-4S] cluster in the late ISC pathway, which is incorporated into various mitochondrial Fe-S proteins (Braymer et al. 2021).

Alternatively, the [2Fe-2S] clusters are exported from mitochondria via the ABC-type transporter Atm1. This export is essential for cytosolic and nuclear Fe-S protein maturation through the CIA machinery (Gerber et al. 2004; Li et al. 2022).

2.3.1 CIA pathway

As mentioned before, the CIA pathway occurs in the cytosol, and it depends on the mitochondrial ISC machinery, which supplies a sulphur-containing intermediate (X-S) or [2Fe-2S] cluster. The exact molecule that is transported to the cytosol is still unknown. This pathway plays a key role in cluster incorporation into cytosolic and nuclear Fe-S apoproteins (*Fig. 2*) (Pandey et al. 2019; Li et al. 2022; Gerber et al. 2004).

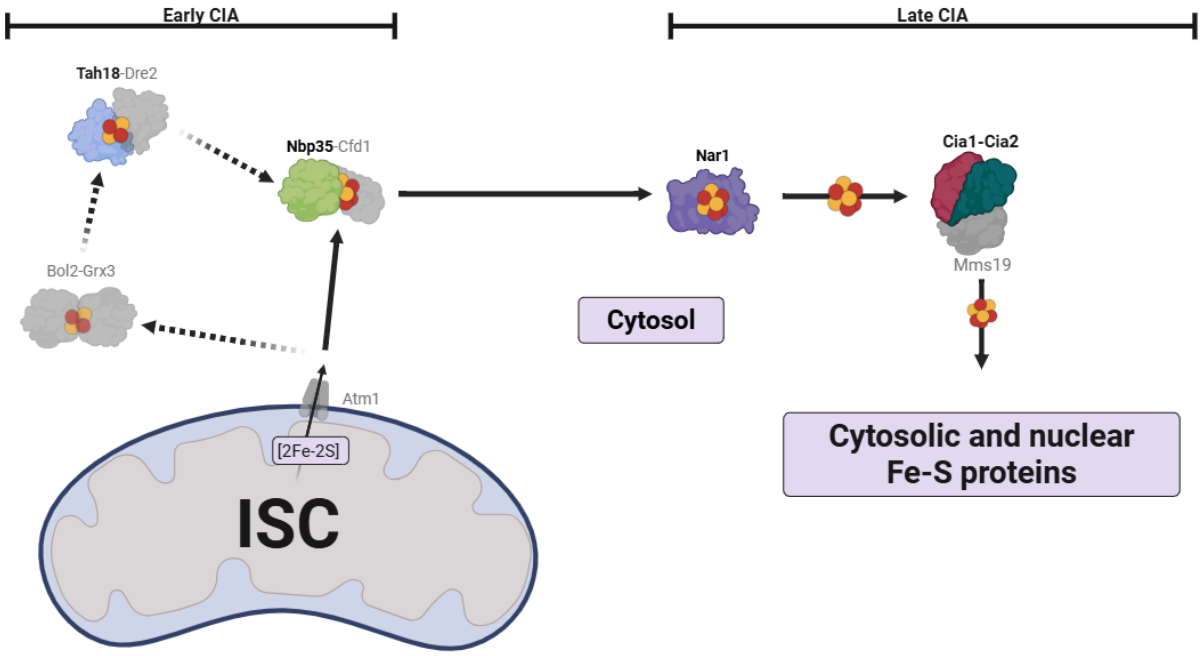

Figure 2: The CIA pathway. Proteins absent in *G. intestinalis* are shown in light grey (BioRender).

The first stage of the CIA pathway involves the assembly of a [4Fe-4S] cluster on a cytosolic scaffold complex formed by a heterodimer of NTPases Cfd1-Nbp35 (Netz et al. 2007). Electron transfer during the cluster formation is facilitated by a NADPH-dependent Tah18-Dre2 complex, where Dre2 contains a [2Fe-2S] cluster, essential for redox-driven biosynthesis (Netz et al. 2010).

In our model organism, the Nbp35 protein expanded into three distinct paralogues, reflecting a unique adaptation of the CIA pathway. Nbp35_1 and Nbp35_2 are localized primarily on the surface of the mitosomes, with a fraction found in the cytoplasm. In contrast, Nbp35_3 was found exclusively in the cytoplasm (Pyrih et al. 2021).

In the pathway Grx3-Bol2 heterodimer is localized upstream of the Nbp35-Cfd1 scaffold and stabilizes [2Fe-2S] clusters using glutathione as a ligand. This complex delivers [2Fe-2S] clusters to the Nbp35-Cfd1 system (Frey et al. 2016).

Following the assembly, the [4Fe-4S] cluster is transferred to the carrier protein Nar1, which plays a bridging role between the scaffold complex and the final delivery system. Both the N- and C-terminus of Nar1 bind the cluster, but only the N-terminal region is able to transfer the [4Fe-4S] cluster to the CIA targeting complex (CTC) (Netz et al. 2007; Urzica et al. 2009).

The final step of the pathway is mediated by the CTC, which includes Mms19, Cia1 and Cia2. The Cia1-Cia2 complex binds to Nar1 via its targeting complex recognition motif (see below). This step allows the complex to receive the cluster from Nar1 (Buzuk et al. 2025). The CTC complex then mediates targeted insertion of the [4Fe-4S] cluster into cytosolic and nuclear apoproteins. Mms19 serves as an adaptor, recognizing specific substrates. Cia1 and Cia2 facilitate the actual delivery of the cluster. In addition, the Cia1-Cia2 complex plays a central role in identifying and binding target apoproteins. The recognition mechanism is based on a targeting complex recognition motif found at the C-terminus of client proteins. This motif contains a conserved sequence of [LIM]-[DES]-[FW]. Structural analyses suggest that CTC complex shows a significant conformational flexibility to accommodate the large distance between the Fe-S cluster and the target site on the apoprotein (Kassube and Thomä 2020; Buzuk et al. 2025).

2.3.2 Fe-S clusters biogenesis in *G. intestinalis*

In *G. intestinalis*, both the ISC and CIA pathways are significantly reduced, reflecting the adaptation to anoxic environment and the presence of the mitosomes instead of a typical mitochondria (Braymer et al. 2021).

The mitosomes of *G. intestinalis* lack DNA, electron transport chain, ATP synthesis machinery and the Krebs cycle. Their only conserved role is the biosynthesis of Fe-S clusters (Jedelský et al. 2011; Tovar et al. 2003). The early ISC pathway is nearly complete, with exception of factors such as Acp1 and Isd11 are missing. Surprisingly, mitosomes of *G. intestinalis* also retain several components of the late ISC pathway, despite the absence of [4Fe-4S] proteins that would normally require these late-acting proteins (Motyčková et al. 2023).

The CIA pathway in our model organism is also highly reduced. Only a minimal set of CIA components is retained: the scaffold protein Nbp35_1-3, the cluster carrier Nar1 and the targeting factors Cia1 and Cia2. Possible orthologs of Tah18 OR1/2 may also be presented (Pyrih et al. 2016).

Notably, *G. intestinalis* also lacks the Atm1 transporter, which exports X-S intermediate or the [2Fe-2S] cluster from mitochondria to the cytosol, leaving the mitosomal-cytosolic connection in cluster biogenesis unresolved (Jedelský et al. 2011; Motyčková et al. 2023).

Altogether, the biogenesis of Fe-S clusters is a highly conserved and essential process across eukaryotes, involving complex machineries in both mitochondria and cytosol. In *G. intestinalis*, this system is remarkably reduced. Despite the simplification, ISC and CIA pathways retain core components, allowing Fe-S clusters biosynthesis.

2.4 Nuclear Fe-S proteins

Although clusters have been associated with mitochondrial enzymes and metabolic processes, it is now known that many essential Fe-S proteins function in the nucleus. They play key role in DNA replication, repair and genome stability. In nuclear enzymes, these clusters serve structural, catalytic and redox-regulatory functions.

An emerging concept is that DNA can act as a conduit for long-range electron transfer, allowing Fe-S clusters to participate in redox signalling. Although still under investigation, this suggests dynamic regulation of DNA-processing enzymes via changing a redox state (Tse et al. 2019).

2.4.1 DNA polymerases

The eukaryotic B-family DNA polymerases δ (Pol δ) and ε (Pol ε) are central to nuclear DNA replication and exhibit a conserved structural organization. Their C-terminal region contains Cys motif that binds a [4Fe-4S] cluster essential for polymerase function (Chanet et al. 2021; Netz et al. 2012).

2.4.1a DNA polymerase δ

DNA polymerase δ (Pol δ) plays a central role in replication of the lagging strand during S-phase and contributes to the synthesis of the leading strand during DNA repair. It is a multi-subunit complex composed of the catalytic subunit and several regulatory subunits that enhance processivity (Kunkel and Burgers 2014).

The catalytic subunit contains a highly conserved motif containing four cysteine residues in its C-terminal domain. It coordinates a [4Fe-4S] cluster, which is required for structural integrity and interaction with other subunits. Loss of the cluster reduces polymerase activity and DNA binding affinity (Jozwiakowski et al. 2019; Netz et al. 2012).

Structural studies show that cluster loss leads to destabilization of the Pol δ, reducing the affinity for DNA template and decreasing the enzymatic activity.

Furthermore, the mutation of cysteine residues in the binding site causes an increasing in replication errors and genomic instability, impaired proofreading capacity, and contribute to cancer development (Shin et al. 2025; Chen et al. 2025; Jozwiakowski et al. 2019). As observed in cryo-EM analysis, Pol δ that lost [4Fe-4S] cluster is unable to effectively bind or synthesize DNA. It underlies the essential role of the cluster in its catalytic activation (Shin et al. 2025).

2.4.1b DNA polymerase ε

DNA polymerase ε (Pol ε) synthesizes the leading strand and possesses 3′-5′ exonuclease proofreading activity. A cysteine-rich motif in its N-terminal catalytic domain coordinates a [4Fe-4S] cluster, which is essential for structural stability, DNA binding and enzymatic activity (Jain et al. 2014; Yuan et al. 2020). Mutations disrupting this motif, for example cysteine to serine substitutions, significantly impair DNA binding, processivity and polymerase activity in Pol ε (Lisova et al. 2022; ter Beek et al. 2019).

Structural and biochemical studies suggest that the [4Fe-4S] cluster acts as a redox-sensitive cofactor. It stabilizes Pol ε-DNA interactions and enables continual synthesis on the leading strand (Netz et al. 2012; Baranovskiy et al. 2018). Loss or oxidation of the cluster impairs DNA synthesis and sensitizes cell to replication stress and genome instability (Moiseeva et al. 2016; Sviderskiy et al. 2020).

2.4.2 Primase

Primase is a DNA-dependent RNA polymerase that initiates DNA replication. It is a key part of the eukaryotic DNA replication system, working as a part of a complex with polymerase α (Pol α). This primase-Pol α complex synthesizes a chimeric RNA-DNA primer. Primase produces a short RNA primer, which is then elongated by a Pol α (Zhang et al. 2014; Smith and Whitehouse 2012).

The primase consists of two subunits: a small catalytic subunit, responsible for *de novo* RNA synthesis, and a large regulatory subunit, which modulates the activity and stability of the complex (Zerbe and Kuchta 2002; Iyer 2005). The large subunit contains a [4Fe-4S] cluster in its C-terminal domain. This cluster plays a regulatory role via redox-dependent control of DNA binding. Specifically, the cluster provides reversible redox switching between oxidized and reduced states. In the oxidized $[4Fe\text{-}4S]^{3+}$ form, the affinity of primase to the DNA template is significantly increased,

promoting stable interaction. In contrast, the reduced [4Fe-4S]$^{2+}$ state exhibits weaker binding, thereby facilitating substrate transfer from primase to Pol α (O'Brien et al. 2017; Sontz et al. 2012).

2.4.3 DNA2 nuclease

DNA2 is a conserved multifunctional nuclease that plays a significant role in the integrity of the genome. DNA2 possesses two activities – ATP-dependent 3′-5′ helicase and 5′-3′ endonuclease activities. These functions are essential for DNA replication and repair and play important role during lagging strand synthesis. It removes the long 5′ flap structures formed during the maturation of Okazaki fragments, thus preventing genomic instability and enabling proper ligation (Burgers and Kunkel 2017; Wu and Brosh 2012).

Besides Okazaki fragment processing, DNA2 plays a critical role in stabilizing replication forks. It contributes to activation of the S-phase checkpoint and facilitates the restart of DNA replication. DNA2 also plays a key role in repairing DNA double-strand breaks by generating 3'-single-stranded DNA tails, working in concert with other nucleases such as EXO1 and the MRN complex. These mechanisms are critical for DNA repair and for protecting chromosomes under the cell stress (Peng et al. 2012; Cejka 2015).

DNA2 contains a [4Fe-4S] cluster at its N-terminal domain. The cluster plays a significant structural and regulatory role. It stabilizes the DNA-binding tunnel along with the interaction between the nuclease and the helicase domains. Mutation of the cysteine residues, which coordinates the cluster, affects both enzymatic activities. It reflects essential role of the cluster within the catalytic process (Pokharel and Campbell 2012; Zhou et al. 2015). Besides this, the [4Fe-4S] cluster has been shown to take part in redox-sensitive DNA binding, suggesting a role in redox signalling and replication fork dynamics (Barton et al. 2019).

2.4.4 Helicases

2.4.4a XPD helicase

Xeroderma pigmentosum group D (XPD) helicase plays a key role in nucleotide excision repair as a part of transcription factor IIH complex (Liu et al. 2008). XPD is a member of the SF2 superfamily and exhibits 5'-3' helicase activity. XPD helicase

contains conserved motif in its N-terminus, including four cysteine residues that coordinate a [4Fe-4S] cluster (Rudolf et al. 2006; Soultanas et al. 2000).

This enzyme comprises four domains: two motor domains, a Fe-S cluster domain and an Arch domain. Together, these elements form a tunnel-like structure, through which ssDNA is threaded during the helicase translocation (Constantinescu-Aruxandei et al. 2016). Motor domains are responsible for ATP binding and hydrolysis, which provide the mechanical energy for DNA translocation (Wu et al. 2009). The Fe-S cluster domain plays a structural role, contributing to the stabilization of the DNA-binding tunnel. The [4Fe-4S] cluster is coordinated by conserved cysteine residues and is essential for maintaining the functional architecture of this enzyme (Constantinescu-Aruxandei et al. 2016). The Arch domain forms a part of DNA translocating tunnel and helps guide ssDNA through the helicase. It also plays role in discriminating between damaged and undamaged DNA (Datta and Brosh 2018).

Mutations in the XPD gene can lead to genetic disorders, including xeroderma pigmentosum, Cocayne syndrome and trichothiodystrophy (Gillet and Schärer 2006).

2.4.4b FancJ helicase

FancJ helicase exhibits both structural and functional similarity to the XPD helicase, including a conserved [4Fe-4S] cluster in its N-terminal domain. It is also involved in DNA repair processes. Mutations in genes encoding FancJ are associated with the development of Fanconi anemia (Rudolf et al. 2006).

2.4.4c RTEL1 helicase

A Regulator of Telomere Elongation Helicase 1 (RTEL1) is a 5′-3′ DNA helicase belonging to the SF2 family. This helicase is essential for telomere length regulation, DNA replication, homologous recombination, and maintenance of genome stability (Landry and Ding 2014).

RTEL1 contains a redox-active [4Fe-4S] cluster in a conserved N-terminal domain, typically coordinated by four cysteine residues. This domain is essential for helicase activity. The cluster modulates a structural conformation of the RTEL1 and its interaction with DNA (White 2009; Landry and Ding 2014).

Helicase unwinds telomeric T-loops and G-quadruplexes, preventing telomere dysfunction and recombination-induced mutations (TERRA). It interacts with telomeric

repeat-containing RNA. This interaction is important for TERRA localization at telomeric ends and contributes to chromatin organization. Disruption of this connection increases TERRA levels and causes telomeric instability (Ghisays et al. 2021).

Mutations in RTEL1 can lead to telomeropathies like Dyskeratosis Congenita and Hoyeraal-Hreidarsson syndrome, characterized by telomere shortering and genomic instability (Ghisays et al. 2021). The [4Fe-4S] cluster is central to RTEL1 function and can be disrupted by oxidative damage, which causes a domain disfunction. It suggests a redox regulation of helicase activity (Landry and Ding 2014).

2.4.5 Glycosylase MUTYH

DNA glycosylase MUTYH plays a central role in the base excision repair (BER) by removing adenine mispaired with 8-oxoguanine, a mutagenic lesion caused by oxidative stress. Its catalytic domain includes a positively charged DNA-binding channel for lesion recognition and contains a [4Fe–4S] cluster, which is essential for DNA binding and redox-based damage detection. Furthermore, MUTYH exhibits DNA-mediated redox activity mediating long-range charge transport signalling (Boal et al. 2007). Mutations in catalytic domain significantly reduce enzymatic activity, showing the critical role of this part of the enzyme (Chepanoske et al. 2000).

Beyond DNA repair, MUTYH also affects cellular senescence. Loss of MUTYH reduces telomeric 8-oxoguanine induced aging, suggesting that MUTYH specifically drives senescence in response to chronic damage, preventing chromosomal instability (De Rosa et al. 2025).

2.4.6 Endonuclease III

As MUTYH, endonuclease III (EndoIII) is also a critical enzyme in BER. It is responsible for identifying and excising oxidized pyrimidines from DNA. EndoIII contains a [4Fe–4S] cluster, which acts a redox-active cofactor (Cunningham et al. 1989; Hassan et al. 2025).

The cluster functions as a redox switch, which modulates the binding affinity to DNA via DNA-mediated charge transport. In its oxidized state, the $[4Fe–4S]^{3+}$ cluster increases DNA binding affinity, allowing the enzyme to scan the genome for damage. If no lesions are detected, the cluster switches to weaker reduced state $[4Fe–4S]^{2+}$,

enabling enzyme to detach. This redox system enables EndoIII to localize DNA damage across whole genome (Hassan et al. 2025).

Conclusion

Fe-S clusters are indispensable cofactors for a wide range of nuclear proteins involved in DNA replication, repair and genomic stability. They play a structural, catalytic and regulatory roles in key enzymes such as DNA polymerases, primase, helicases, nucleases and glycosylases. Disruption or oxidation of Fe-S clusters often leads to impaired DNA processing and increased genomic instability, highlighting their critical role in enzymes.

3 Aims of the work

Aim of this work is to characterize the role of selected proteins from the CIA pathway during the formation of Fe-S clusters on the nuclear proteins in the anaerobic parasite *G. intestinalis*.

Specific aims:

1) Identification of a nuclear Fe-S protein for functional analysis of the CIA pathway in *G. intestinalis*.
2) Generation of knock-out mutants of selected CIA pathway components.
3) Phenotypic analysis of a knock-out cell line lacking nucleotide binding protein 35 (ΔNbp35_3).

4 Materials and methods

4.1 Organisms, their cultivation and transformation

4.1.1 Escherichia coli

Chemically competent *Escherichia coli* strain TOP10 (Thermo Fisher Scientific) was used for plasmid propagation.

4.1.1a Cultivation

The cultures were cultivated in LB medium at 37°C overnight (ON) on shaker (220 rpm). Ampicillin (Sigma) was used at a final concentration of 100 µg/ml to select bacteria containing the desired plasmid.

4.1.1b Transformation

Bacteria were transformed with plasmid using the heat shock method. An aliquot of 150 µl of chemically competent *E. coli* was mixed with 1 µl of plasmid DNA or 10 µl of ligation reaction (see below) and incubated on ice for 20 minutes. Then the cells were placed into a heating block set to 42°C for 45 seconds and immediately returned to ice for 2 minutes. After the heat shock, 300 µl of S.O.C. medium was added, and the cells were incubated for 1 hour at 37°C on shaker (220 rpm). Following the recovery, bacteria were plated on LB agar plates with ampicillin (Sigma, 100 µg/ml) and incubated overnight at 37°C in a microbiological incubator.

4.1.2 Giardia intestinalis

All experiments described in this work were conducted using the wild-type *Giardia intestinalis* WBc6 (ATCC 50803) cell line and its laboratory-derived variants. All manipulations were carried out under sterile conditions in a laminar flow cabinet.

4.1.2a Cultivation

Axenic cultures were cultivated under microaerobic conditions – in tightly closed 8 ml glass tubes filled to the top with TYI-S-33 medium - at 37°C in a thermostat. *G. intestinalis* forms a confluent monolayer along the wall. The cultures were passaged every 3-4 days. For passaging, dead cells settled at the bottom of the tubes were removed using a Pasteur pipette, and the tubes were placed on ice for 10 minutes to

detach adherent trophozoites. Approximately 200-300 µl of the cell suspension was transferred into fresh medium with or without selection antibiotics, depending on the experiment.

Table 1: Selection antibiotics and final concentrations

Geneticin (G418)	600 µg/ml
Puromycin (PUR)	50 µg/ml
Blasticidin (BLAST)	75 µg/ml

If a monolayer did not form after 3-4 days, the culture medium was replaced.

4.1.2b Transfection via electroporation

G. intestinalis cells were cultured in 50 ml culture flasks in TYI-S-33 medium. After 2 days of cultivation cell monolayer was formed. The medium was removed, and cells were washed with ice-cold sterile PBS. Flasks were incubated on ice for 20 minutes to detach the cells. The cells were then pelleted by centrifugation at 1200 x *g* for 10 minutes at 4°C and resuspended in 500 µl of TYI-S-33 medium.

Cell density was determined using a Beckman cell-counter after 1:1000 dilution. The suspension was adjusted to a final concentration of $3.3*10^7$/ml. For electroporation, 300 µl of the cell suspension was transferred to a 0.4 cm electroporation cuvette, followed by addition of 50 µg of the plasmid DNA. The suspension was gently mixed and incubated on ice for 10 minutes.

Electroporation was performed using Bio-Rad Gene Pulser under the following conditions: 350 V, 1000 µF and 750 Ω resistance. After electroporation, the cuvettes were returned to ice for 5 minutes. The transfected cells were then transferred to a 16 ml culture tubes containing TYI-S-33 medium and incubated at 37°C in a thermostat.

On the following day, the culture medium was exchanged, and selection antibiotics were added depending on the experiment (*Tab. 2*).

Table 2: Selection antibiotics and concentrations

Geneticin (G418)	150 µg/ml
Puromycin (PUR)	25 µg/ml
Blasticidin (BLAST)	75 µg/ml

Then the culture medium was refreshed every third day until the cells formed a monolayer. At that point, the concentration of the selection antibiotic was increased as stated above (*Tab. 1*).

4.1.2c Subcloning

Single-cell subcloning was performed to obtain clonal populations of *G. intestinalis*. Cultures were first incubated on ice for 20 minutes. Subsequently, 200 µl of TYI-S-33 medium with the appropriate antibiotics was added to each well of 96-well plates. Single-cell sorting was performed using the BD FACS Aria Fusion flow cytometer (Imaging Methods Core Facility, BIOCEV), with one cell dispensed per well. The plates were then hermetically sealed in plastic bags together with Oxoid AnaeroGen sachets (Thermo Fisher Scientific) to establish anaerobic conditions. Oxoid Resazurin Anaerobic Indicators were included to verify anaerobiosis during incubation. After 4-7 days of incubation, clonal cell populations were identified by light microscopy and transferred to 8 ml screw-cap glass culture tubes containing TYI-S-33 medium with selection antibiotics.

4.1.2d Long-term storage

For long-term storage, *G. intestinalis* cultures were preserved in liquid nitrogen (-196°C) with 5% dimethyl sulfoxide as a cryoprotectant. For recovery, frozen cells were thawed and transferred into a cultivation tube containing fresh TYI-S-33 medium and incubated for 1-2 hours. To remove residual dimethyl sulfoxide, the medium was exchanged after incubation and selection antibiotics were added.

4.2 Solutions and cultivation media

LB medium (Bertani 1951)

Composition	Quantity
LB Broth (Lennox)	20 g/l

Sterilise by autoclaving

S.O.C. medium (Hanahan 1983)

Composition	Quantity
Tryptone (Oxoid)	20 g/l
Yeast Extract (Oxoid)	5 g/l
NaCl (Sigma-Aldrich)	10 mM
KCl (Sigma-Aldrich)	2.5 mM
Glucose (Sigma-Aldrich)	20 mM
$MgCl_2$ (Sigma-Aldrich)	10 mM
$MgSO_4$ (Sigma-Aldrich)	10 mM

pH=7, sterilise by autoclaving, store in -20°C

TYI-S-33 medium (Keister 1983)

Composition	Quantity / Concentration
Trypticase Peptone (Oxoid)	20 g/l
Yeast Extract (Oxoid)	10 g/l
NaCl (Lachner)	5 g/l
K2HPO4 (Sigma-Aldrich)	1 g/l
Glucose (Sigma-Aldrich)	10 g/l
KH_2PO_4 (Sigma-Aldrich)	0.6 g/l
L-cysteine × H_2O (Sigma-Aldrich)	2 g/l
L-ascorbic acid (Sigma-Aldrich)	0.2 g/l
Ammonium ferric citrate (Sigma-Aldrich)	28 mg/l
Adult or Fetal Bovine serum (Gibco)	10%
Bile bovine	0.1%
Penicillin-Streptomycin (Sigma-Aldrich)	10 000 U/ml, 10 000 µg/ml

pH=6.8, sterilise by Filter Steritop 0.22 µm (Millipore), store in -20°C

PBS

Composition	Concentration
NaCl (Sigma-Aldrich)	137 mM
KCl (Sigma-Aldrich)	2.7 mM
Na_2HPO_4 × 12 H_2O (Sigma-Aldrich)	10 mM
KH_2PO_4 (Sigma-Aldrich)	1.8 mM

pH=7-7.4, sterilise by autoclaving

Blotting buffer

Composition	Volume
10x Tris/Glycine/SDS buffer (BioRad)	100 ml
Methanol (Lach-Ner)	200 ml
dH_2O	700 ml

Blocking buffer

Composition	Concentration
Low fat dry milk (NutriStar)	5%
Tween 20	0.25%
PBS	

Ponceau S solution

Composition	Concentration
Ponceau S (Merck)	5 g/l
Acetic acid	1%

2x PEM buffer

Composition	Concentration
PIPES (Sigma-Aldrich)	20 mM
EGTA (Sigma-Aldrich)	2 mM
$MgSO_4$ (Sigma-Aldrich)	0.2 mM

pH=6.9, sterilise by autoclaving, store in -20°C

PEMBALG buffer

Composition	Concentration
Bovine Serum Albumin (Sigma-Aldrich)	1%
L-lysine (Sigma-Aldrich)	100 mM
Gelatine (Sigma-Aldrich)	0.5%
2x PEM buffer	

Store in -20°C

4.3 Used antibodies

- Rat monoclonal anti-HA primary antibody (Roche)
- HRP-conjugated anti-rat secondary antibody (Sigma-Aldrich)
- Alexa Flour 488-conjugated anti-rat secondary antibody (Thermo Fisher Scientific)

4.4 Plasmids

4.4.1 pONDRA

The plasmid pONDRA (*Fig. 3*) was used to generate episomal overexpression constructs. The coding sequence of the selected nuclear protein was cloned into the plasmid, with a C-terminal double hemagglutinin (HA) tag. The plasmid also carries antibiotic resistance genes: ampicillin (AMP) for bacterial selection and G418 for selection in *G. intestinalis*.

Figure 3: pONDRA plasmid with introduced coding sequence of GL50803_2340 as an example.

4.4.2 pGdelP_PaqCI

The pGdelP_PaqCI plasmid (*Fig. 4*) was used for the gene knockout of *Nbp35_3* (GL50803_0015324). This vector contains restriction sites for the PaqCI enzyme, enabling efficient cloning of guide RNA (gRNA) spacer sequences specific to the *Nbp35_3* gene. It also carries a deletion cassette flanked by homologous sequences 5´ untranslated region (UTR) (upstream) and 3´UTR (downstream) of *Nbp35_3* locus. These UTRs mediate targeted integration into the genome via homologous recombination. The plasmid includes antibiotic resistance genes: ampicillin (AMP) for bacterial selection and PUR for selection in *G. intestinalis*.

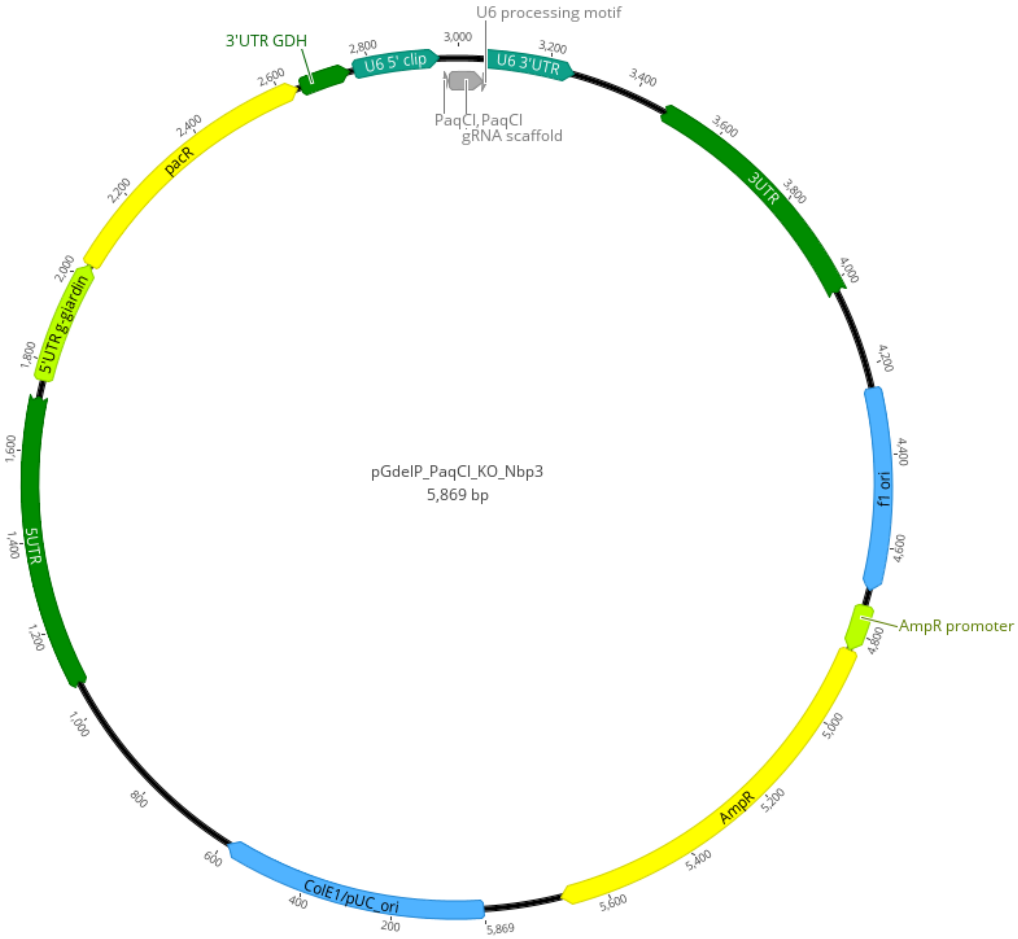

Figure 4: pGdelP_PaqCI plasmid with introduced 5´UTR and 3´UTR of Nbp35_3 gene (dark green) and gRNA (grey).

4.5 Methods

4.5.1 Construct preparation

4.5.1a Gene amplification

The UTRs of Nbp35_3 were amplified by polymerase chain reaction (PCR) using Q5 polymerase from genomic DNA of the *G. intestinalis* WBc6 (ATCC 50803) cell line, purified with the E.Z.N.A. Tissue DNA Kit. (*Tab. 3, 4*). For this purpose, specific forward (fwd) and reverse (rev) primers were designed (Sigma-Aldrich) (*Tab. 5*).

Table 3: Q5 PCR reaction

Component	Volume	Final concentrations
Q5 High-Fidelity DNA Polymerase (NEB)	0.5 µl	0.02 U/µl
5X Q5 Reaction Buffer (NEB)	10 µl	1x
fwd primer (10µm)	2.5 µl	0.5 µM
rev primer (10µm)	2.5 µl	0.5 µM
10mM dNTPs (Fermentas)	1 µl	200 µM
Template DNA	1 µl	< 1,000 ng
dH_2O	32.5 µl	

Table 4: Q5 PCR program

Temperature	Time	Step
98°C	30 s	Initial Denaturation
98°C 50-72°C 72°C	10 s 30 s 30s/kbp	30 Cycles
72°C	2 minutes	Final Extension
4°C	∞	Hold

Table 5: The primers used for amplification

***Nbp35_3* (GL50803_0015324)**	**Sequence (5´-3´)**
3´UTR fwd (ApaI)	AAAGGGCCCGTGACGTTTGATGGTCTGC
3´UTR rev (XbaI)	AAATCTAGAGACCAGTCTTCAAAGTGTGA
5´UTR fwd (AscI)	AAAGGCGCGCCGGTCTGGTTTGCAGAGAT
5´UTR rev (AvrII)	AAACCTAGGTTATTTTCTCTGTGGTTGTATACC

The PCR product was separated by horizontal gel electrophoresis on a 1% agarose gel. The gel was stained with SYBR Safe (Invitrogen) to enable visualization under UV light using a UV Transilluminator (Syngene). GeneRuler DNA Ladder Mix (Thermo Fisher Scientific) was used as the molecular weight standard. For sample loading, 6× TriTrack DNA Loading Dye (Thermo Fisher Scientific) was used. The desired DNA fragment was then excised from the gel and purified using the E.Z.N.A. Gel Extraction Kit (Omega Bio-Tek).

4.5.1b Restriction

The amplified DNA fragments and the plasmid backbone were digested using restriction enzymes (New England BioLabs) specific to each construct design. Restriction enzymes and their corresponding reaction buffers (New England BioLabs) were selected according to the requirements of each insert and plasmid, following the manufacturer's recommendations to ensure optimal activity (*Tab. 6*). The volume of plasmid DNA used in each reaction was calculated to ensure a total of 10 µg DNA per reaction (*Tab. 7*). Restriction reactions were incubated in a thermoblock at 37 °C for 2 hours, or at 16 °C ON.

Table 6: List of the restriction enzymes and reaction buffers

Restriction reaction	**Restriction enzymes**	**Reaction buffer**
Nbp35_3 5´UTR	AscI, AvrII	rCutSmart
Nbp35_3 3´UTR	ApaI, XbaI	rCutSmart

Table 7: Overview of restriction reaction composition

Component	Amount
Plasmid	
Plasmid DNA	10 µg
Restriction enzyme 1	1 µl
Restriction enzyme 2	1 µl
Reaction buffer	5 µl
dH_2O	up to 50 µl
Insert	
PCR product	30 µl
Restriction enzyme 1	1 µl
Restriction enzyme 2	1 µl
Reaction buffer	5 µl
dH_2O	up to 50 µl

Following digestion, reaction products were separated by horizontal agarose gel electrophoresis in 1% agarose gels prepared in TAE buffer. DNA bands of the expected size were visualized under UV light and excised from the gel. DNA fragments were isolated using the E.Z.N.A. Gel Extraction Kit (Omega Bio-Tek, USA).

4.5.1c Ligation

Purified and digested DNA fragments and plasmids were ligated using T4 DNA ligase (ThermoFisher, USA) (*Tab. 8*). The ligation reaction was incubated ON at 16 °C.

Table 8: The composition of restriction reaction

Component	Volume
Plasmid	200 ng
Insert	at a molar ratio 5:1
T4 DNA ligase	1 µl
T4 DNA ligase buffer (10x)	2 µl
dH_2O	up to 25 µl

4.5.1d Cloning of gRNA

gRNAs complementary to the gene of interest were designed using the EuPaGDT online tool (http://grna.ctegd.uga.edu/). For each target, a pair of complementary oligonucleotides was constructed. Cloning overhangs (CGGC and AAAC) were added to facilitate integration into the plasmid (*Tab. 9*).

Table 9: Oligomer pairs for gRNA targeting the *Nbp35_3*

Oligonucleotide name	Sequence (5´-3´)
Nbp35_3 gRNA 175_fwd	CGGCACGAGGAGCATGCTCTAGCCG
Nbp35_3 gRNA 175_rev	AAACCGGCTAGAGCATGCTCCTCGT
Nbp35_3 gRNA 891_fwd	CGGCGTGGCGTCAAGAAGATGTGTG
Nbp35_3 gRNA 891_rev	AAACCACACATCTTCTTGACGCCAC
Nbp35_3 gRNA 872_revcom_fwd	CGGCATCACTGGCCTTTGTGAGTTG
Nbp35_3 gRNA 872_revcom_rev	AAACCAACTCACAAAGGCCAGTGAT

Subsequently, the oligonucleotides were diluted to 100 µM in dH_2O. The annealing reaction was then prepared (*Tab. 10*). Annealing was performed by incubation at 95 °C for 5 min, followed by gradual cooling to room temperature over 2.5 hours to ensure proper hybridization of the oligonucleotides.

Table 10: Composition of the annealing reaction

Component	Volume
dH_2O	14 µl
Forward oligonucleotide (100 µM)	2 µl
Reverse oligonucleotide (100 µM)	2 µl
10x T4 ligase buffer	2 µl

For the cloning reaction (*Tab. 11*), annealed oligonucleotides were ligated into the plasmid. The digestion-ligation reaction was incubated at 37 °C for 2 hours followed by 65 °C for 10 min to inactivate the ligase and restriction enzymes.

Table 11: Composition of the cloning reaction

Component	Volume
dH_2O	13,5 µl
NEBuffer rCutSmart	2 µl
Plasmid (100 ng/µl)	1 µl
Annealed gRNA oligonucleotides	1 µl
PaqCI enzyme	1 µl
PaqCI activator	0,5 µl
T4 ligase	1 µl

Following ligation, competent *E. coli* cells were transformed. Subsequently, cells were plated on LB agar with AMP (30 µg/ml) and incubated overnight at 37 °C. Several colonies then were tested by PCR (see Chapter 4.5.1e). The remainder of each positive bacterial suspension was grown in 5 ml LB medium with AMP at 37 °C overnight with shaking (220 rpm). Plasmid DNA was isolated using a E.Z.N.A. Plasmid DNA Mini Kit I (Omega Bio-Tek). Verification of the cloned gRNA was performed by sequencing (see Chapter 4.5.1f).

4.5.1e PCR testing of *E. coli* clones

A colony was picked with a pipette tip and resuspended in 50 µl of dH_2O. To lyse the bacterial cells and release plasmid DNA, 10 µl of the suspension was transferred into PCR tubes and placed in a thermal cycler. The program "Crack" was used for the cell lysis (*Tab. 12*).

Table 12: "Crack" program

Temperature	Time
94 °C	180 s
50 °C	180 s
94 °C	180 s
45 °C	180 s
94 °C	180 s
4 °C	∞

The lysates were subsequently used as templates in PCR reactions prepared with EmeraldAmp PCR Master Mix (Takara Bio, Japan) and specific primers (10 µM, 0.5 µl). The gRNA sequencing primer (5′-GGTGCATGACCCGCAAGC-3′) was used as the forward primer, while the reverse primers are listed in Table 9. The thermal cycling conditions are shown in Table 13.

Table 13: Emerald PCR program

Temperature	Time	Cycles
98°C	3 min	1
98°C 55-65°C 72°C	10 s 30 s 1 min/kbp	30
72°C	2 minutes	1
4°C	∞	

PCR products were resolved by horizontal electrophoresis on 1% agarose gels and visualized under UV illumination.

4.5.1f DNA sequencing

gRNA testing

Sanger sequencing was performed in 8 µl reactions containing 5 pmol of a T7 prom-long primer (5´- GTAATACGACTCACTATAGGGC - 3´) and template DNA adjusted to 3 ng/100 bp. The reaction was completed with nuclease-free water. Sequencing reactions were submitted to an OMICS-Genomics Laboratory at BIOCEV. The results were analysed using Geneious Prime software (versions 2024.0 and 2025.1.3).

Nbp35_3 knock-out in *G. intestinalis*

Sanger sequencing was also employed for detection of the changes in the *Nbp35_3* gene in a knock-out cell line. To cover the whole length of the gene, two independent sequencing reactions were performed using primers shown in a table (*Tab. 14*).

Table 14: Primers used for *Nbp35_3* sequencing

Name	Sequence 5´-3´
Nbp35_3_control_F	CAACCTCTATTCCCATGCGCG
Nbp35_3_control_R	GAATGCATCATACCCAGGTG

4.5.2 *G. intestinalis* DNA, RNA isolation and cDNA synthesis

To isolate genomic DNA from *G. intestinalis*, E.N.Z.A. Tissue DNA Kit (Omega Bio-Tek) was used.

To confirm the deletion of the *Nbp35_3* in the knock-out cell line, PCR was performed using cDNA as a template. Total RNA was extracted from fully grown cultures using High Pure RNA Isolation Kit (Roche). Genomic DNA was removed by adding 5 µl of 10× MgCl2 reaction buffer and 1 U/µl of DNase I (Thermo Fisher Scientific). After 30 minutes of incubation at 37°C, enzymes were inactivated by 5 minutes of heating at 65°C with adding of 3 µl of 50mM EDTA.

cDNA was synthesized using the SuperScript III Reverse Transcriptase kit (Invitrogen) with oligo$(dT)_{10}$ primers. The reaction was incubated at 50°C for 30 minutes and inactivated at 70°C for 15 minutes.

The presence of the *Nbp35_3* transcripts was tested using gene specific primers (*Tab. 15*). *Beta-giardin* gene (GL50803_004812) was used as a positive control. PCR was performed with Q5 program.

Table 15: Primers used for *ΔNbp35_3* testing

Name	Sequence 5´-3´
Nbp35_3_cDNA_F	CATGTTGTGGTGGTGGTAGC
Nbp35_3_cDNA_R	GAATGCATCATACCCAGGTG
Beta-giardin_F	CAAGGATATCCATATGTCTCTTGACGCCGAAGCACGA
Beta-giardin_R	CAAGACGCGTGTGCTTTGTGACCATCGAGA

4.5.3 Sodium dodecyl sulfate polyacrylamide gel electrophoresis (SDS-PAGE)

SDS-PAGE was performed to analyse protein expression in *G. intestinalis*. Cultures (8 ml) were harvested at confluence. Culture tubes were placed on ice for 20 minutes. Cells were pelleted by centrifugation at 1200 x g for 10 minutes at 4°C, washed once in 1 ml of cold sterile PBS, and transferred to microcentrifuge tubes. A

second centrifugation step under the same conditions was performed and resulting pellets were resuspended in SDS sample buffer. Samples were denatured by heating at 95°C for 10 minutes and stored at -20°C prior to gel electrophoresis.

Protein separation was performed on vertical polyacrylamide gels, consisting of 15% resolving gel overlaid with a 5% stacking gel. Tris-Glycine-SDS buffer was used as the running buffer. 15 µl of denatured lysates were loaded alongside 5 µl of PageRuler Plus Prestained Protein Ladder (Thermo Fisher Scientific), which served as a molecular weight reference. Electrophoresis was initiated at 100 V until proteins migrated into the resolving gel. After, the voltage was increased to 180 V and maintained until the sample approached the bottom of the gel.

4.5.4 Western blotting

Proteins separated by SDS-PAGE were transferred onto a nitrocellulose membrane using a blotting system (Biometra Fastblot). Prior to assembly, the nitrocellulose membrane, gel and filter papers were incubated in blotting buffer to ensure proper wetting and to prevent air bubbles during transfer. The blotting “sandwich” was assembled on the anode of the blotting apparatus in the following order: filter paper, nitrocellulose membrane, SDS-PAGE gel, filter paper. Excess buffer was carefully removed to avoid current leakage. The cathode was placed over the “sandwich”. Protein transfer was performed for 1 hour at a constant current, calculated as 1.5 mA per cm^2 of gel area.

Following blotting, the nitrocellulose membrane was stained with Ponceau S solution to visualize the transferred proteins. The membrane was subsequently blocked to prevent nonspecific binding by incubation in blocking buffer for 1 hour at RT on a rocking platform.

The membrane was then incubated with the primary rat monoclonal anti-HA antibody diluted 1:1000 in blocking buffer for 1 hour at RT or ON at 4°C with gentle agitation. Afterward, the sample was washed three times with blocking buffer for 10-20 minutes each on a rocker. Subsequently, the membrane was incubated with an appropriate HRP-conjugated secondary antibody diluted 1:2000 in blocking buffer. This was followed by two washes with blocking buffer and a final wash in PBS with 0,25% Tween 20, each for 10-20 minutes on a rocking platform. The signal was developed by applying 500-800 µl of Immobilon Crescendo Western HRP substrate (Millipore)

directly onto the membrane and visualized using Amersham Imager 600 (GE Healthcare, USA).

4.5.5 Immunofluorescence microscopy of *G. intestinalis*

Trophozoites were fixed by adding paraformaldehyde (Electron Microscopy Sciences) directly to the growing culture to reach a final concentration of 1%. The samples were incubated for 30 minutes at 37 °C in a microbiological incubator. After fixation, the cells were pelleted by centrifugation at 900 x g for 5 minutes at 4 °C. The supernatant was discarded, and the cells were washed in 1 ml of PEM buffer under the same centrifugation conditions. The cells were then resuspended in PEM buffer at a ratio of 150 µl per coverslip.

Coverslips were covered with 5 µl poly-L-lysine solution (Sigma-Aldrich) and dried. Subsequently, 100 µl of the cell suspension was placed on the coverslips and incubated for 15 minutes at RT to promote cell adhesion. Excess suspension was removed, and the coverslips were gently dried using a stream of air.

Cell permeabilization was performed by incubating the coverslips in 0.1% Triton X-100 (Sigma-Aldrich) for 10 minutes at RT. Afterward, the samples were washed three times in PEM buffer for 10 minutes. To block nonspecific binding sites, the coverslips were incubated in PEMBALG blocking buffer for 30 minutes at RT.

For immunostaining, the samples were incubated with the rat monoclonal anti-HA antibody diluted in PEMBALG (1:1000) for 1 hour at RT. Subsequently, coverslips with the cells were incubated with Alexa Fluor 488 (Thermo Fisher Scientific) diluted in PEMBALG (1:1000) for 1 hour at RT in the dark. Afterward, the samples were washed three times in PEM buffer for 10 minutes.

DNA counterstaining and mounting were performed by applying 20 µl of VECTASHIELD Antifade Mounting Medium with DAPI (Vector Laboratories) directly onto the samples. The coverslips were carefully mounted on the slides and sealed using nail polish.

Fluorescence microscopy was performed using a Nikon Eclipse Ti-S inverted confocal microscope fitted with a 100x oil immersion objective. Images processing and analysis were carried out using Fiji software (version 1.53c) (Schindelin et al. 2012).

4.5.6 Enzymatic activity assay

The following chemicals were prepared for the enzymatic assay (*Tab. 16*):

Table 16: chemicals used for enzymatic activity assay

Chemical	Concentration
KH_2PO_4 buffer (Penta), pH 7.4	100 mM
Methyl viologen (Sigma-Aldrich)	100 mM
Coenzyme A (CoA) (Cayman)	8.6 mM
Pyruvic acid sodium salt (Sigma-Aldrich)	715 mM
Triton X-100 (Sigma-Aldrich)	1%
β-Mercaptoethanol (Sigma-Aldrich)	14.3 M

G. intestinalis trophozoites were cultivated into 75 cm^2 culture flasks. After a confluent monolayer had formed, the growth medium was replaced with cold PBS, and the culture flasks were incubated on ice for 20 minutes. Subsequently, the cells were harvested by centrifugation at 1200 x g for 10 minutes 4 °C and supernatant was discarded. The pellet was then washed in 1 ml of PBS and resuspended in 1 ml of PBS. To normalize the samples, dilution was performed based on optical density measurement, followed by a third centrifugation step under identical conditions. Then, pellet was resuspended in 300 µl PBS supplemented with 0.6 µl of the protease inhibitors TLCK (10 µl) and leupeptin (10 µl).

Prior to use, KH_2PO_4 buffer was deoxygenated by sparging with N_2 for 30 minutes. The assay was performed in an anaerobic cuvette with three chambers.

To the main chamber were added:

2 ml of KH_2PO_4 solution

30 µl of methyl viologen

20 µl of pyruvic acid sodium salt

50 µl of CoA

20 µl of β-Mercaptoethanol

Subsequently, one of the smaller chambers was loaded with 20 µl Triton X-100, while varying volumes (8–30 µl) of the prepared cell suspension were placed into the second chamber. After adding all components, the mixture was deoxygenated by sparging with N_2 for 5 minutes. Following incubation, the contents of the smaller

chambers were released into the main chamber to initiate the reaction. Absorbance at 600 nm was monitored using UV-2600 UV-VIS spectrophotometer (Shimadzu, JPN).

4.5.7 Measurement of protein concentration

The protein concentration was measured using the Bicinchoninic Acid (BCA) Kit for Protein Determination. A standard curve was prepared by adding BSA (1 mg/ml) to a 96-well plate in the following volumes (µl):

0	2.5	6.25	12.5	18.75	25

and adjusting the volume to 25 µl with dH_2O. To the designated wells, 2, 4, or 8 µl of the cell suspension were added and brought to a final volume of 25 µl with dH_2O. The BCA working solution was prepared by mixing BCA with 4% $CuSO_4 \times 5H_2O$ in a 50:1 ratio, and 200 µl of this mixture was added to each well. The plate was incubated at 60 °C for 15 minutes. Absorbance of the standards and samples was measured at 562 nm using the Synergy H1 multi-mode reader (Omega Bio-Tek, USA), and protein concentrations were calculated from the standard curve.

5 Results

5.1 Identification of a nuclear Fe-S proteins

5.1.1 Bioinformatic prediction of nuclear Fe-S proteins

To identify candidate nuclear Fe-S proteins in *G. intestinalis*, we analysed the whole proteome using the MetalPredator tool (https://metalweb.cerm.unifi.it/tools/metalpredator/), which predicts proteins containing Fe-S clusters based on known amino acid sequence motifs. Protein localization was then predicted using DeepLoc-2.0 (https://services.healthtech.dtu.dk/services/DeepLoc-2.0/) and complemented with data from other organisms (*Tab. 17*). Based on this combined approach, eight putative nuclear Fe-S proteins were selected (*Tab. 18*). Most of these candidates are enzymes involved in DNA metabolism, including DNA replication, repair, or transcription regulation.

Control nuclear proteins were selected according to previous studies (McInally et al. 2019) (*Tab. 18*). These proteins are localized in the nucleus but do not contain Fe-S clusters.

Table 17: The predicted Fe-S proteins in *G. intestinalis*

Gene	Name	Localization
GL50803_6175	Nitroreductase family protein	Cytosol
GL50803_3042	Hybrid cluster protein lateral transfer candidate	Cytosol
GL50803_7662	RNase L inhibitor	Cytosol
GL50803_22677	Nitroreductase Fd-NR2	Cytosol
GL50803_10329	Ferredoxin Fd3	Cytosol
GL50803_6304	Fe-hydrogenase-1	Cytosol
GL50803_17063	Pyruvate-flavodoxin oxidoreductase	Cytosol
GL50803_114609	Pyruvate-flavodoxin oxidoreductase	Cytosol
GL50803_7195	Glutamate synthase	Cytosol
GL50803_9662	Ferredoxin Fd1, Fd2	Cytosol
GL50803_15090	L-serine dehydratase	Cytosol
GL50803_16519	AstB/chuR-related protein	Cytosol
GL50803_24662	L-serine dehydratase	Cytosol
GL50803_9368	Pyruvate-formate lyase-activating enzyme	Cytosol
GL50803_4248	Diphthamide biosynthesis protein 1	Cytosol
GL50803_16125	Glycerol-3-phosphate dehydrogenase	Cytosol
GL50803_4081	hypothetical (4Fe-4S binding domain-containing protein)	Cytosol
GL50803_23325	hypothetical (4Fe4S Ferredoxin)	Cytosol

GL50803_0060379	Ferredoxin Fd1, Fd2	Cytosol
GL50803_14604	Nucleotide-binding protein 1	Cytosol CIA
GL50803_15324	Nucleotide-binding protein 1	Cytosol CIA
GL50803_10969	Nucleotide-binding protein 1	Cytosol CIA
GL50803_33030	Nar1	Cytosol CIA
GL50803_14821	IscA (HesB domain-containing protein)	Mitosome
GL50803_14519	IscS	Mitosome
GL50803_27266	Fdx ([2Fe-2S] ferredoxin)	Mitosome
GL50803_2013	Grx5 (Glutaredoxin-related protein)	Mitosome
GL50803_15196	IscU (NifU-like protein)	Mitosome
GL50803_32838	Nfu1	Mitosome
GL50803_0060288	BolA	Mitosome
GL50803_10055	DNA-directed RNA polymerase subunit D	Nucleus
GL50803_6980	DNA polymerase/primase	Nucleus
GL50803_4328	TFIIH basal transcription factor complex helicase subunit	Nucleus
GL50803_5631	TFIIH basal transcription factor complex helicase subunit	Nucleus
GL50803_102963	tRNA 2-methylthioadenosine synthase	Nucleus
GL50803_35094	DNA polymerase delta, catalytic subunit	Nucleus
GL50803_92673	CHL1-like protein/Rad3-related DNA helicase	Nucleus
GL50803_16639	Histone acetyltransferase Elp3	Nucleus
GL50803_27326	DNA polymerase alpha subunit A	Nucleus
GL50803_7474	DNA-directed RNA polymerase RPB3	Nucleus
GL50803_16463	O-sialoglycoprotein endopeptidase	Nucleus

Table 18: Putative nuclear Fe-S proteins and controls

Controls		**Size**
GL50803_21201	mRNA decapping protein	29 kDa
GL50803_2340	Its NLS was used to target Cas9 to nucleus	17 kDa
Fe-S proteins		
GL50803_5631	TFIIH basal transcription factor complex helicase subunit	117 kDa
GL50803_7474	DNA-directed RNA polymerase subunit RPB3	36 kDa
GL50803_10055	DNA-directed RNA polymerase subunit D	37 kDa
GL50803_102963	tRNA 2-methylthioadenosine synthase	58 kDa
GL50803_6980	DNA polymerase/primase	60 kDa
GL50803_92673	CHL1-like protein/Rad3-related DNA helicase	90 kDa
GL50803_16639	Histone acetyltransferase Elp3	65 kDa
GL50803_16463	O-sialoglycoprotein endopeptidase	26 kDa

5.1.2 Overexpression of potential nuclear Fe-S proteins

To generate *G. intestinalis* cell lines overexpressing genes encoding putative nuclear Fe-S proteins, the plasmid pONDRA with the gene sequences and C-terminal double HA tag was used. These constructs were kindly generated and provided by Martin Benda.

The plasmids were transfected into the *G. intestinalis* WBc6 cell line by electroporation. Following transfection, the cultures were selected in growth medium supplemented with G418. Once stably growing monolayers of transfected cells were established, cell lysates were prepared to verify expression of the genes.

Protein expression was analysed by SDS-PAGE followed by Western blotting. A rat monoclonal anti-HA antibody was used as the primary antibody, and an HRP-conjugated anti-rat secondary antibody was applied for detection. Signal was visualized using an Amersham Imager 600 system (*Fig. 5*). Samples 10055, 16463, and 102963 exhibited bands corresponding to the expected size. However, they also showed a high number of non-specific degradation products. In contrast, two control samples 20201 and 2340 and two predicted Fe-S proteins 6980 and 7474 displayed clear bands of the expected size with only a minimal presence of non-specific degradation products.

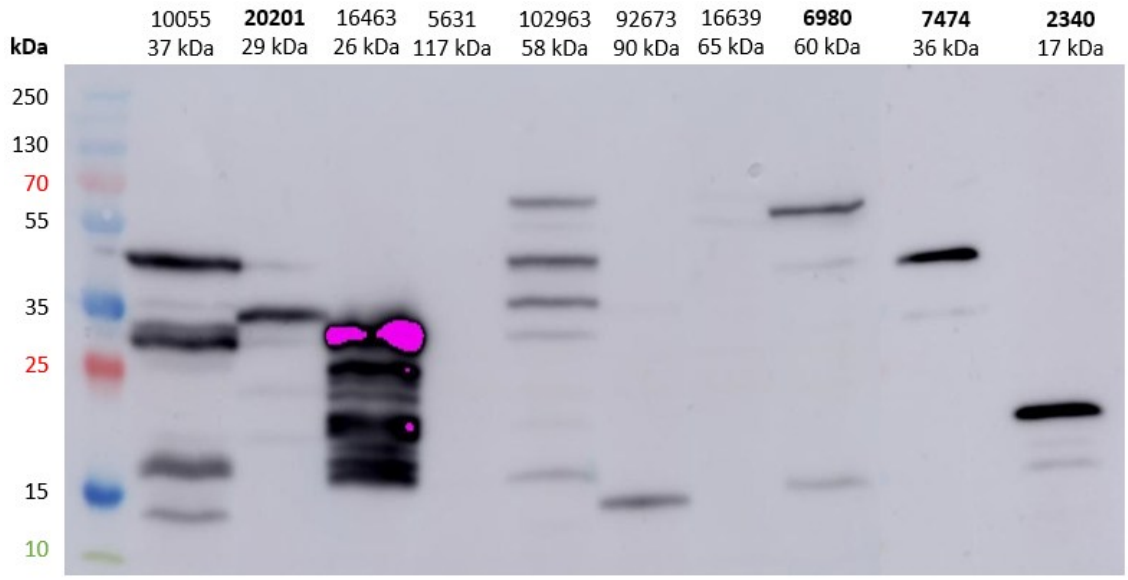

Figure 5: Verification of protein expression in *G. intestinalis* cells. The gene names of the predicted nuclear Fe-S proteins and their corresponding expected molecular sizes are on the top of the picture. Western blot analysis of *G. intestinalis* samples. Samples 10055, 16463, and 102963 show bands of the expected size along with numerous non-specific degradation products. In contrast, control samples 20201 and 2340, 6980, 7474 display clear bands at the expected size with minimal non-specific degradation.

5.1.4 Localization of potential nuclear Fe-S proteins

To determine the localization of the overexpressed proteins, we performed immunofluorescence microscopy on *G. intestinalis* cells using a rat monoclonal anti-HA

antibody and a fluorescently conjugated secondary antibody (ALEXA 488). A fluorescent signal was detected in approximately 5–40% cells, depending on the expressed protein. Although the nuclear localization was expected, the majority of tested proteins were detected predominantly in the cytosol. However, for proteins 2340 and 7474 we observed both cytosolic and nuclear localization (*Fig. 6*).

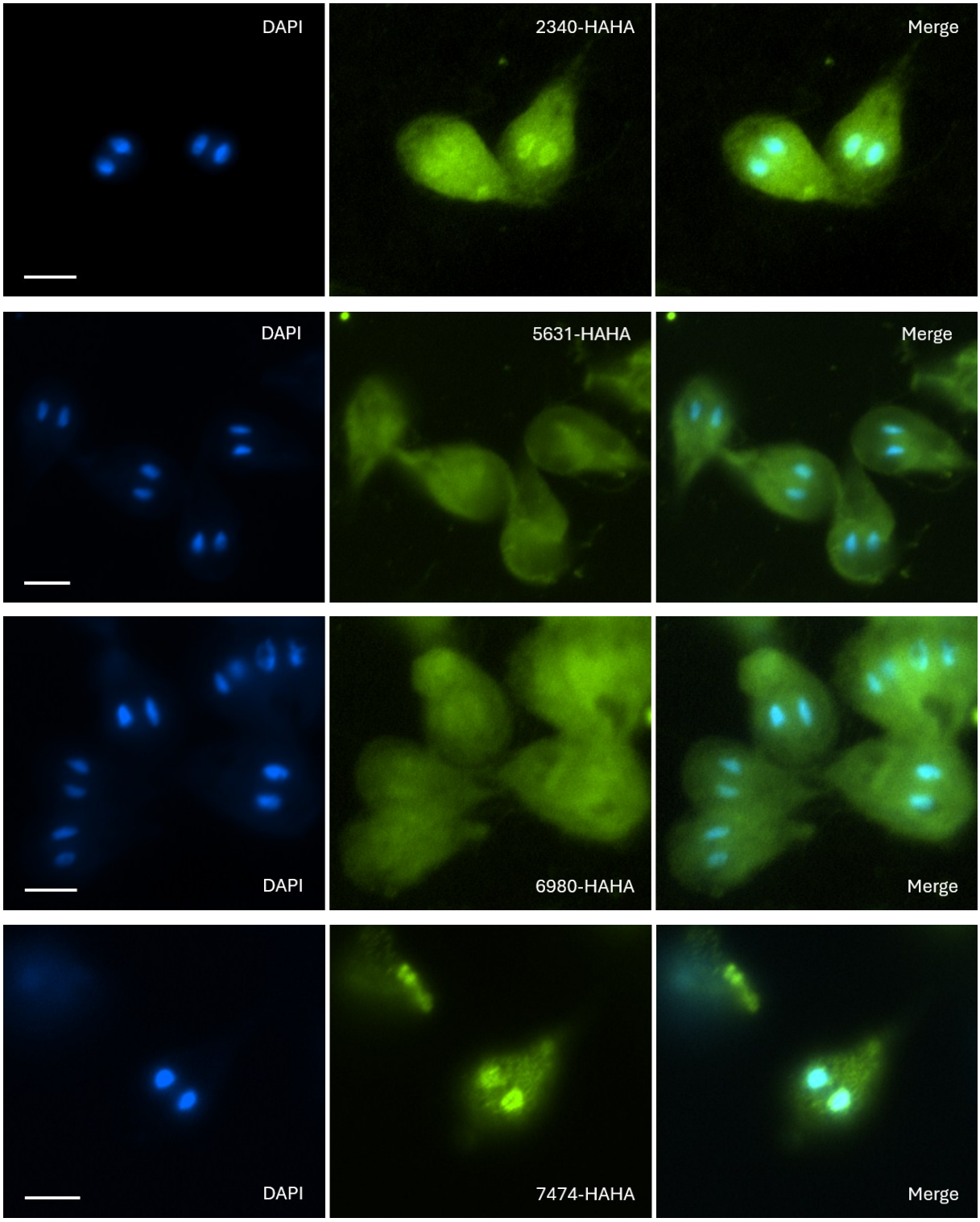

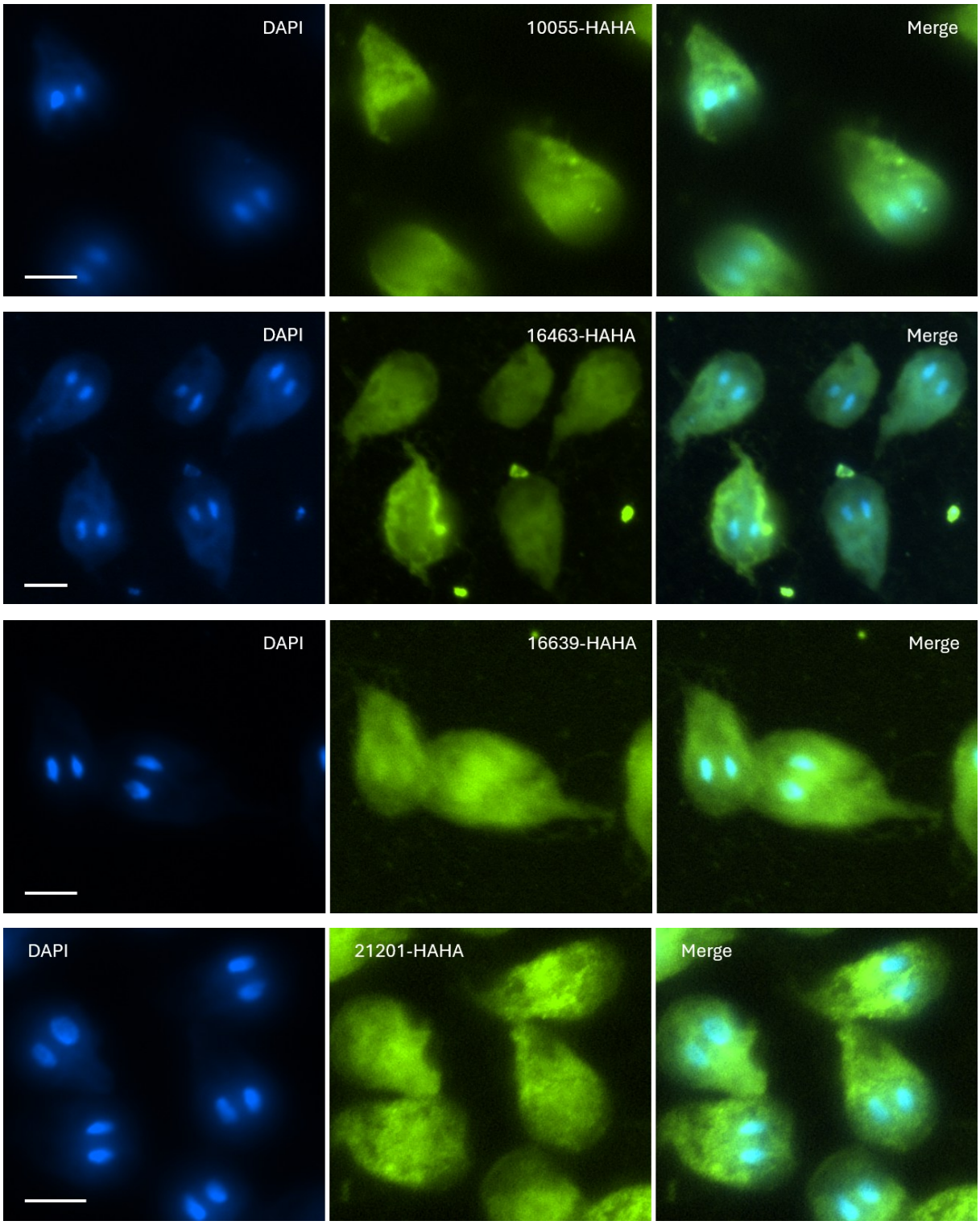
DAPI
10055-HAHA
Merge
DAPI
16463-HAHA
Merge
DAPI
16639-HAHA
Merge
DAPI
21201-HAHA
Merge

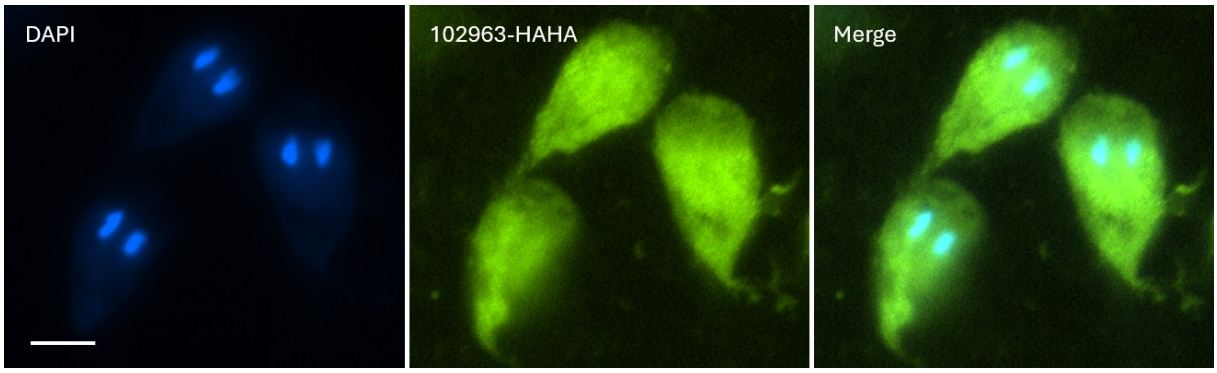

Figure 6: Localization of potential nuclear Fe-S proteins. Immunofluorescence micrographs of *G. intestinalis* cells stained with DAPI (blue) and labelled with a rat monoclonal anti-HA antibody (green). The merged images show predominantly cytosolic localization for most tested proteins, while proteins 2340 and 7474 exhibit both cytosolic and nuclear localization. Scale bar: 5 µm.

In summary, we successfully identified the putative Fe-S nuclear protein DNA-directed RNA polymerase subunit RPB3 (GL50803_7474) as a marker for molecular analysis of the CIA pathway.

5.2 Knock-out of the CIA pathway protein Nbp35_3

Initially, we planned to generate knock-outs of all known genes of proteins involved in the CIA pathway. However, upon identifying that a knock-out of *Nbp35_3* had already been obtained, we decided to continue our work with this cell line.

5.2.1 Constructs preparation

For the knock-out of the *Nbp35_3* gene, two pGdelP_PaqCI plasmids with inserted 5´UTR and 3´UTR were prepared. The integration cassette contained a single gRNA, which differed between the two constructs. Each gRNA, referred to as 175 and 891 gRNA, targeted the Nbp35_3 protein coding sequence at a different site of the coding sequence. Correct insertion of the DNA fragments into the plasmids was confirmed by sequencing.

5.2.2 Knock-out generation and confirmation

For this experiment, the *G. intestinalis* WBc6 cell line expressing a HA-tagged Cas9 endonuclease (WBc6-Cas9) was used. To introduce the plasmids into *G. intestinalis*, transfection by electroporation was employed. The cultures were maintained in the presence of selective antibiotics to promote the integration of the

cassette. After *G. intestinalis* formed a confluent monolayer along the wall of culture tube, subcloning was performed using flow cytometry with a cell sorter. Successful subcloning was achieved only in the 175-gRNA cell line, whereas the 891-gRNA cell line failed to grow in the 96-well plate.

To confirm the integration of the cassette, PCR was performed using forward primer annealing downstream of the *Nbp35_3* gene and a reverse primer annealing within the integrated cassette. To assess the presence of the original gene, the same forward primer was used in combination with a reverse primer annealing within the *Nbp35_3* coding region (*Fig. 7*).

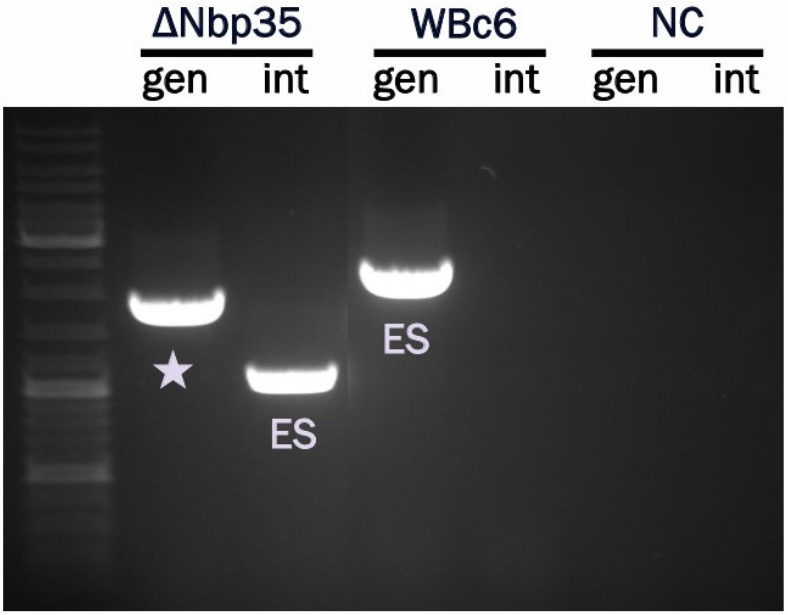

Figure 7: The results of the PCR screening of the Nbp35_3 knock-out cell line. The genomic DNA was isolated from the Nbp35_3 knock-out cell line and tested for the presence of the Nbp35_3 gene (gen), the integration of the deletion cassette (int). Genome of a WBc6 cell line (WBc6) and dH_2O (NC) were used as a control. ES – expected size of the band. ★ – different size than expected. The PCR products were separated by horizontal 1 % agarose gel electrophoresis.

The PCR result demonstrated both the integration of the deletion cassette and the presence of the *Nbp35_3* gene in the knock-out cell line. However, the band corresponding to the *Nbp35_3* gene was noticeably shorter than that observed in the wild-type WBc6 cell line.

Based on these results, we decided to sequence the generated PCR product to determine the changes that occurred in the *Nbp35_3* gene (*Fig. 8*). The results show a deletion of 202 base pairs within the coding region of *Nbp35_3*. This deletion disrupts the open reading frame, likely resulting in non-functional protein synthesis or complete

loss of protein expression. Based on these results, we conclude that the *Nbp35_3* gene has been inactivated in the knock-out cell line.

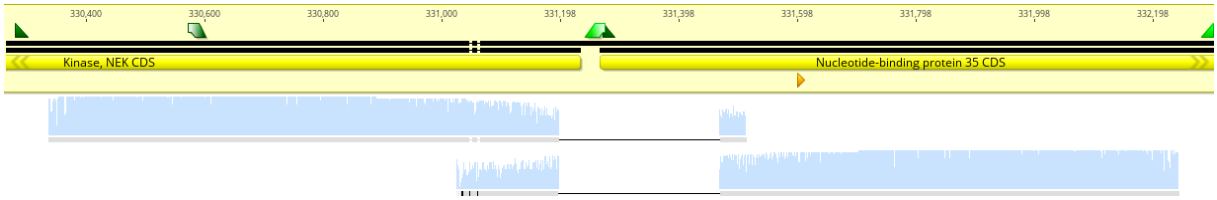

Figure 8: *ΔNbp35_3* sequencing results. The sequencing results of the mutated gene indicate the absence of a 202 bp fragment in the Nbp35_3 gene in the knock-out cell line.

Total RNA was then isolated from the clonal population. Part of the isolated total RNA was reverse transcribed to obtain cDNA, while the remaining RNA was retained as a negative control. Subsequently, DNA, cDNA and RNA samples were analysed for the presence of *Nbp35_3* gene by PCR amplification using primers specific to the Nbp35_3 coding sequence. *Beta-giardin* gene was used as a reference control (*Fig. 9*). These results confirm that the *Nbp35_3* gene has been successfully deleted at the genomic level and is not transcribed in the knock-out line. This suggests a complete loss of *Nbp35_3* expression.

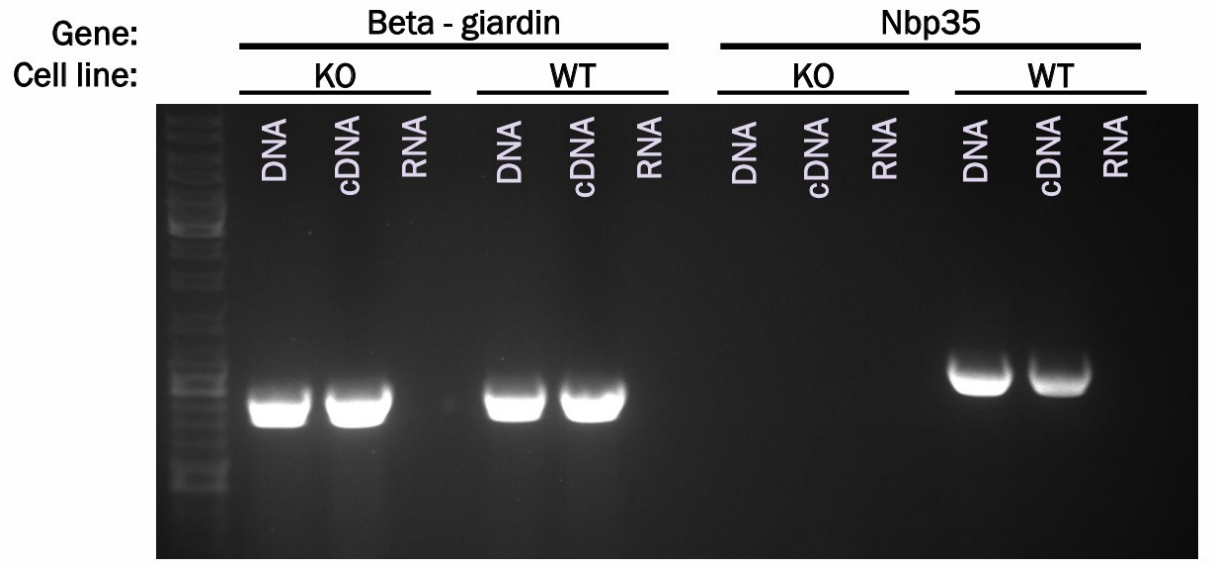

Figure 9: The results of the PCR analysis of DNA, cDNA and RNA of the Nbp35_3 in the knock-out cell line. The PCR results confirmed the absence of the Nbp35 gene in both the genomic DNA and cDNA of the knockout line. The PCR products were separated in 1 % agarose gel.

In summary, the *Nbp35_3* gene was successfully disrupted in *G. intestinalis* using a CRISPR/Cas9 with 175-gRNA. Integration of the deletion cassette and removal of a 202 bp fragment within the *Nbp35_3* coding sequence were confirmed by PCR and sequencing analyses. Furthermore, PCR screening of genomic DNA and reverse-transcribed cDNA verified the loss of *Nbp35_3* expression in the knock-out line, indicating effective gene disruption at both the genomic and transcript levels.

5.3 Phenotypic analysis of *ΔNbp35_3* cell line

5.3.1 Mass spectrometry proteomic profiling

To assess whether the knock-out of *Nbp35_3* affected the overall gene expression in *G. intestinalis*, a mass spectrometry-based proteomic analysis was performed. Cell pellets from the WBc6 and *ΔNbp35_3* cell lines were prepared and sent for analysis to the OMICS Mass Spectrometry Core Facility at BIOCEV. The acquired data were subsequently analysed.

Prior to analysis, all variant surface proteins (VSPs) were excluded from the data due to natural expression variability during cultivation. As expected, the absence of Nbp35_3 in the knockout cell line was confirmed. Additionally, a membrane protein encoded by the gene GL50803_0017350 was found to be absent in the knockout cell line. This protein is annotated as a hypothetical product in *G. intestinalis*, but homology analysis suggests it may belong to the rhomboid-like or related derlin family. To visualize the differences in protein abundance, volcano plot was generated (*Fig. 10*) using VolcaNoseR (https://huygens.science.uva.nl/VolcaNoseR/). Differential expression analysis revealed that 53 proteins were significantly upregulated, and 28 proteins were downregulated in the *ΔNbp35_3* cell line compared to the wild type. Selected proteins such as PFOR, three subunits of the AP-2 complex and TFIIH P34 are highlighted in the volcano plot. These proteins were selected for annotation because they are predicted to be dependent on the CIA pathway or are likely to be indirectly affected by the absence of *Nbp35_3*.

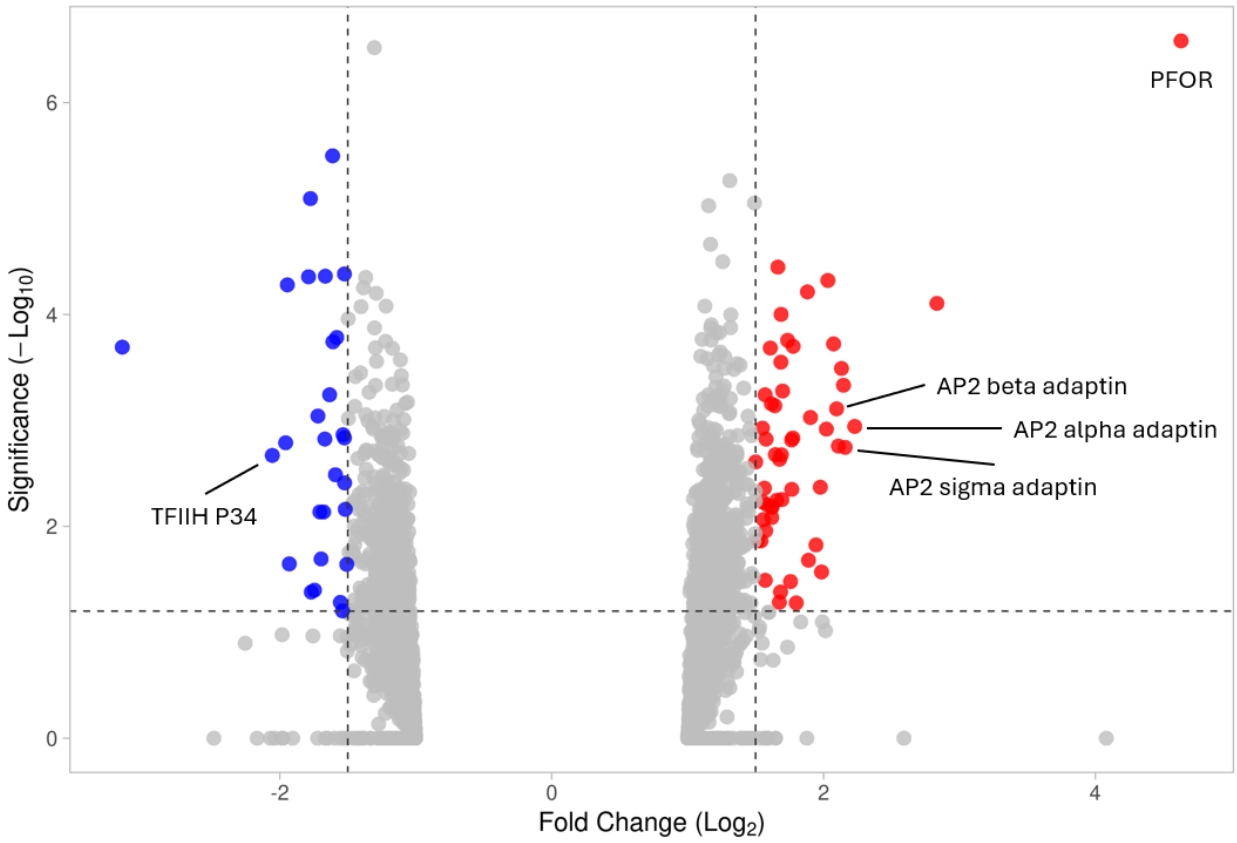

Figure 10: Volcano plot showing differential expression of 3719 proteins in the *G. intestinalis*. ΔNbp35_3 cell line. Selected proteins with significant fold changes are highlighted. Increased expression was observed for PFOR (GL50803_00114609, Fold Change = 4.63) and three of the four subunits of AP-2 complex: α-adaptin (GL50803_0017304, Fold Change = 2.02), β-adaptin (GL50803_0021423, Fold Change = 2.13), and σ-adaptin (GL50803_005328, Fold Change = 2.16). Decreased expression was observed for TFIIH P34 (GL50803_0013512, Fold Change = -2.06). Significance threshold is 1.2.

Proteomic profiling revealed significant changes in the abundance of proteins involved in redox metabolism, transcription, and membrane trafficking. These findings support the essential role of *Nbp35_3* in maintaining cellular homeostasis through the maturation of Fe-S proteins.

5.3.2 PFOR activity

Based on the analysis of the mass spectrometry results, we decided to measure the enzymatic activity of PFOR spectrophotometrically. The activity was determined in the WBc6 (n=3) and ΔNbp35_3 (n=3) cell lines and subsequently compared. The activity assay was performed in a single biological triplicate (*Plot 1*). A reduction in PFOR activity was observed in the *ΔNbp35_3* cell line (0.432 µmol/min/mg) compared

to the wild-type WBc6 (0.646 µmol/min/mg), corresponding to a 33.2% decrease. However, statistical analysis using an independent samples t-test revealed that this difference was not statistically significant (p = 0.080). These results suggest a possible impairment of Fe-S cluster-dependent enzymatic activity.

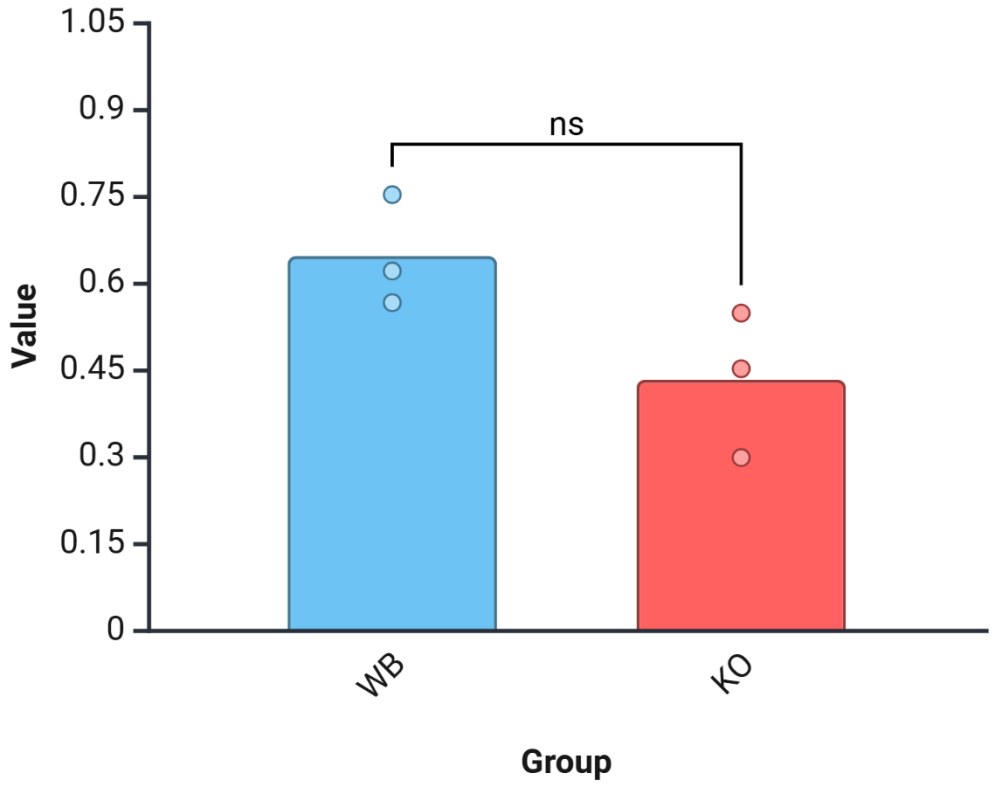

Plot 1: Comparison of PFOR enzymatic activity between WBc6 and ΔNbp35_3. A reduction of PFOR activity was observed in ΔNbp35_3 (0.432 µmol/min/mg) compared to WBc6 (0.646 µmol/min/mg). The measurement was performed in a triplicate. The data set was statistically tested. An independent samples t-test indicated a non-significant effect of Group: p = 0.080.

In conclusion, we observed the absence of Nbp35_3 in the knock-out cell line at the protein level, as revealed by mass spectrometry. Also, the knock-out led to marked changes in the proteomic profile, including increased abundance of PFOR and several subunits of the AP-2 complex. Despite the elevated PFOR protein levels, the enzymatic activity assay indicated a reduced specific activity of PFOR in ΔNbp35_3 compared to the WBc6 cell line.

6 Discussion

This study was divided into three main parts, each designed to contribute to understanding of the CIA pathway in *G. intestinalis*: 1) Identification of nuclear Fe-S proteins; 2) Knock-out of the CIA pathway proteins; 3) Phenotypic analysis of ΔNbp35_3 cell line.

6.1 Identification of nuclear Fe-S proteins

Nuclear Fe-S proteins play a crucial role in DNA replication, repair and maintenance of genome stability. The presence of Fe-S clusters in nuclear proteins can support more diverse roles than just classic redox functions. They are essential for enzymatic activity, structural integrity or redox sensing. However, in many cases, their function in nuclear proteins is still not fully understood (Lill 2009). The existing research suggests that these cofactors may play broader regulatory roles, which makes them valuable targets for future studies.

This part of the thesis focused on identifying suitable nuclear Fe-S proteins whose maturation depends on the CIA pathway downstream of the mitosomal ISC pathway. These proteins could serve as potential experimental markers for the future studies of the ISC and CIA pathways in *G. intestinalis*. Given that *G. intestinalis* lacks respiratory chain and the majority of „classical aerobic" metabolism in the mitosomes, which are dominant acceptors of Fe-S clusters. It represents an excellent model system to study nonmitochondrial assembly and transport of the clusters. *G. intestinalis* energy metabolism strongly depends on the activity of "anaerobic" cytosolic Fe-S proteins such as PFOR, ferredoxins and hydrogenase, whose maturation has also not been studied in any eukaryotic system. To further investigate how Fe-S clusters are maturated and delivered into nuclear proteins in an anaerobic eukaryote, we first needed to identify a Fe-S protein with nuclear localization.

Initially, a bioinformatic analysis was performed to identify potential candidate proteins. Based on this analysis, ten proteins were selected for subsequent characterization. Among them, two proteins served as a control, as their nuclear localization was experimentally confirmed, but they lack a Fe-S cluster in their structure (*Tab. 18*) (McInally et al. 2019).

To experimentally test the nuclear localization of the selected proteins, we generated cell lines with episomal expressed gene copies. According to the results of

protein expression verification, we chose four of the ten proteins: two controls: 20201 and 2340 and two predicted Fe-S proteins: 6980 and 7474 (*Fig. 5*). In samples 10055, 1646 and 102963 clear bands corresponding to the expected molecular size were detected, indicating the presence of the correct product. However, in addition to the specific bands, a substantial number of non-specific bands was also observed. These additional bands are likely to represent degradation products, which could result from two experimental reasons: (1) overexpression of the target nuclear protein, resulting in abnormally high protein levels which may trigger degradation of these products, and (2) interference from the HA-tag, which could affect the folding or protein stability. In contrast, in samples 5631 and 16639 no detectable bands were observed, indicating either very low expression level or a protein stability issue. In addition, in sample 92673 a single band was detected, although its size was significantly smaller than expected.

Fluorescence microscopy was used to study the subcellular localization of the overexpressed proteins across ten different samples. Notably, nuclear localization was observed in only two samples: 2340 (control) and 7474 (DNA-directed RNA polymerase subunit RPB3), while the remaining proteins localized to the cytosol.

Possible explanation is that DNA or RNA metabolizing proteins can functionally shuttle between the nucleus and cytoplasm or the episomal expression generates an excess of the nuclear protein that is actively exported to the cytosol. It is also possible that the presence of the HA-tag masks the nuclear localization signal, which may reduce the efficiency of nuclear import. These results highlight how cells control protein localization, especially when experimentally manipulated. To avoid these issues, *in situ* tagging of the protein can be used, which maintains expression at endogenous levels. Additionally, to prevent the masking of the nuclear localization signal, placing the tag at the N-terminus would be an alternate solution.

According to obtained data, subunit RPB3 of DNA-directed RNA polymerase II (GL50803_7474) was selected as a molecular marker for analysis of the CIA pathway and other future experiments. RPB3 contains a [4Fe-4S] cluster and functions as a scaffolding subunit that initiates the assembly of the RNA polymerase II complex through the formation of a heterodimer with RPB11 (Benga 2005). Initially, we also planned to combine the knock-out of the Nbp35_3 with the overexpression of RPB3 to determine the impact of the CIA pathway defect on nuclear Fe-S proteins. The planned approach involved measuring the incorporation of ^{55}Fe into the target protein. Mutant and control cells would be incubated with ^{55}Fe, followed by pull-down using the HA-tag.

The level of incorporated iron would then be analyzed by scintillation counting or detecting the radioactive signal on a native gel. However, this part of the experiment could not be performed due to the time limitation. It will be important to complete these studies in the future.

6.2 Knock-out of the CIA pathway proteins

The CIA pathway in *G. intestinalis* is very reduced compared to other eukaryotes. Our model organism lacks the Atm1 transporter, which links the ISC pathway with the CIA machinery by X-S or [2Fe-2S] export. The CIA pathway includes the scaffold protein Nbp35, the cluster carrier Nar1, and the targeting factors Cia1 and Cia2. In addition, electron transfer protein Tah18 may also be present. *G. intestinalis* lacks Bol2-Grx3 complex, Dre2 and Mms19 from the CTC (Pyrih et al. 2016; Motyčková et al. 2023). Together, these data suggest that *G. intestinalis* contains highly reduced pathway for the cytosolic Fe-S cluster assembly or possibly, other yet unknown lineage-specific proteins participate in this process.

The second part of the thesis aimed to dissect the functional importance of individual components of the CIA machinery. To achieve this, we attempted targeted knock-outs of the genes encoding proteins of interest. The generation of these knock-out lines was essential for assessing the impact of CIA component disruption on the phenotype of *G. intestinalis*.

At the beginning of the project, we aimed to generate knock-out for all genes of proteins involved in the CIA pathway, including Tah18, three paralogues of Nbp35, Nar1, Cia1 and Cia2. For each gene, three different knock-out constructs were designed and prepared. Despite these efforts, the only successful knock-out we generated was one of the three paralogs of Nbp35. This protein was previously localized to the cytosol, while the other two paralogues showed both mitosomal and cytosolic localization (Pyrih et al. 2021). We hypothesize that *G. intestinalis* possesses three Nbp35 paralogues because each one may act as a specific carrier for a different subset of cytosolic or nuclear Fe-S target proteins. The inability to generate knock-out cell lines for other CIA components suggests that these proteins are essential for *G. intestinalis* viability. Their complete removal likely leads to the absence of Fe-S clusters in essential nuclear or cytosolic proteins which is incompatible with the cell survival. Some of the other putative knock-out cell lines, including *ΔNar1* and *ΔCia1*, were able

to survive only for a few generations. They never formed a complete monolayer, and the cultures died out after several passages. In future experiments, we will attempt to establish conditional knock-out strategy for these genes or establish cells line with only partial deletion of four gene alleles.

In the case of Nbp35_3, it is possible that complete removal of the gene was possible because the other Nbp35 paralogs are at least partially redundant and may compensate for of the loss of one variant (Pyrih et al. 2021). Alternatively, the target Fe-S proteins that are dependent on the activity of Nbp35_3 are not essential for *G. intestinalis* survival.

6.3 Phenotypic analysis of *ΔNbp35_3* cell line

The third part involved the analysis of the *ΔNbp35_3* mutant cell line, as this was the only viable knock-out we were able to obtain. The observed phenotype provided insights into the biological role of Nbp35_3 in our model organism.

To analyse phenotypic changes in the *G. intestinalis* knock-out lines, mass spectrometry analysis was performed. Initially, we expected to observe alterations in the expression of nuclear and cytosolic proteins containing Fe-S clusters. The results of our study revealed the following findings:

1) A decrease in the expression of subunit P34 of the transcription factor TFIIH (GL50803_0013512, Fold Change = -2.06). The TFIIH complex is essential for RNA polymerase II transcription initiation and nucleotide excision repair. The P34 subunit serves as a scaffold within the core complex (Zachayus et al. 2025). Although this subunit does not contain a cluster itself, the TFIIH complex includes the XPD helicase, which harbours a [4Fe-4S] cluster (Kuper et al. 2014). Therefore, the knock-out may have an indirect effect on the structure and function of this complex.

2) An increase in the expression of three out of four subunits of the adaptor protein complex 2 (AP-2) was detected: α-adaptin (GL50803_0017304, Fold Change = 2.02), β-adaptin (GL50803_0021423, Fold Change = 2.13), and σ-adaptin (GL50803_005328, Fold Change = 2.16). AP-2 is a heterotetrameric complex functions as a clathrin adaptor during clathrin-mediated endocytosis

and encystation. It links cargo proteins at the plasma membrane to the clathrin coat that drives vesicle formation (Collins et al. 2002). The upregulation of these subunits in the knock-out line may indicate a cellular response to Fe-S cluster deficiency. It is likely that the cell activates endocytosis as a compensatory mechanism to increase iron uptake and restore Fe-S cluster biogenesis.

3) An increased expression level was observed for PFOR-2 (GL50803_00114609, Fold Change = 4.63). This cytosolic protein contains three [4Fe-4S] clusters that play a key role in electron transfer (Chabrière et al., 1999). The upregulation of this enzyme may indicate that, in the absence of Fe–S clusters, PFOR-2 becomes less functionally active, prompting the cell to increase its expression to compensate for reduced enzymatic efficiency. It is possible that Nbp35_3 specifically participates in the biosynthesis of clusters to PFOR-2, as the expression levels of other Fe-S-containing proteins, and specifically of the other PFOR gene (PFOR-1), remained unchanged. This observation may suggest a specialized functional relationship between Nbp35_3 and PFOR-2 in *G. intestinalis*.

Subsequently, we measured the enzymatic activity of PFOR in both the WBc6 and ΔNbp35_3 cell lines (*Plot 1*). Pyruvate was used as a substrate, methyl viologen as an electron acceptor. WBc6 shows a PFOR activity 0.646 µmol/min/mg of protein, which corresponds to the wild-type enzymatic determined activity in previous work (Townson et al. 1996) (0.612 µmol/min/mg of protein). ΔNbp35_3 cell line showed a 33% reduction in PFOR activity (0.432 µmol/min/mg of protein). However, an independent samples t-test indicated that this difference was not statistically significant. The lack of statistical significance may be attributed to the limited number of biological replicates (n=3) used in the assay, yet a clear trend toward decreased activity was observed. In future experiments, we plan to include more biological replicates to improve statistical power.

It is important to note, that the total PFOR activity measured in our assay represents combined enzymatic activities of PFOR-1 and PFOR-2. As a consequence, we cannot determine whether the observed activity changes are specific to PFOR-1, PFOR-2 or both.

Based on the data, three possible interpretations of the observed phenotype related to PFOR are suggested:

1. ΔNbp35_3 cells reduce activity of both PFOR isoforms: There is a defective delivery of Fe-S cluster to both PFORs in the ΔNbp35_3 cell line, and the cell responses (for yet unknown reason) only via upregulating the expression of PFOR-2.

2. ΔNbp35_3 cells reduce activity only of PFOR-1: There is a defective delivery of Fe-S cluster only to PFOR1 and the cells respond vis compensatory upregulation of PFOR-2 expression. This cellular response reflects an attempt to restore pyruvate decarboxylation and maintain energy metabolism by increasing the expression of an alternative isoform with overlapping function.

3. ΔNbp35_3 cells reduce activity of PFOR-2: The absence of functional PFOR-2 activity may trigger a compensatory increase in the expression of its gene. This represents a cellular rescue mechanism aimed at restoring metabolic function. However, if the enzyme remains inactive due to cofactor deficiency, increased expression alone may not be sufficient to recover enzymatic activity.

In future work, PFOR-1 and PFOR-2 may be distinguished based on their substrate specificity. PFOR-1 is suggested to be strictly specific for pyruvate, while PFOR-2 may metabolize other substrates (Townson et al. 1996). This difference can be accessed via *in vitro* enzyme assays using pyruvate or other oxoacids (ketobutyrate, oxalacetate) as a substrate. Alternatively, the presence of clusters in the two PFORs can be detected using ^{55}Fe labelling of Fe-S proteins and their separation on native protein electrophoresis, since the two enzymes exhibit different mobilities in the gel.

7 Conclusion

This study investigated the role of CIA pathway proteins in the biogenesis of Fe-S clusters on cytosolic and nuclear proteins in *G. intestinalis*, which has a highly reduced form of mitochondria called mitosome. Through a combination of bioinformatic prediction and overexpression analyses, we identified subunit RPB3 of DNA-directed RNA polymerase (GL50803_7474) as a suitable nuclear Fe-S protein marker.

We also successfully generated a gene knock-out of the CIA protein Nbp35_3 using CRISPR/Cas9 and confirmed the loss of its transcript and protein product. Proteomic analysis of the ΔNbp35_3 cell line revealed shifts in protein abundance, including decreased level of TFIIH P34 (GL50803_0013512), increased levels of three of the four AP-2 complex subunits: α- (GL50803_0017304), β- (GL50803_0021423), σ- (GL50803_005328) adaptins and PFOR-2 (GL50803_00114609). Interestingly, although PFOR protein levels were elevated, its enzymatic activity declined, indicating that Fe-S cluster biogenesis defects may uncouple protein expression from functional capacity.

Overall, our findings confirm that the CIA machinery in *G. intestinalis* plays an essential role in cellular Fe-S protein maturation. The results underscore the protist's evolutionary adaptation to an anaerobic lifestyle while retaining a functionally critical Fe-S assembly system.

8 List of Abbreviations

AMP – ampicillin
AP-2 – adaptor protein complex 2
BCA – bicinchoninic acid
BER – base excision repair
CIA – cytosolic iron-sulphur cluster assembly
CoA – coenzyme A
CTC – CIA targeting complex
EndoIII – endonuclease III
Fe-S cluster – iron-sulphur cluster
fwd – forward
G418 – geneticin
gRNA – guide RNA
HA – hemagglutinin
HRP – horseradish peroxidase
ISC – iron-sulphur cluster assembly
NOR – nitric oxide reductase
ON – overnight
PBS – Phosphate-Buffered Saline
PCR – polymerase chain reaction
PFOR – pyruvate:ferredoxin oxidoreductase
Pol – polymerase
PUR – puromycin
rev – reverse
RT – room temperature
RTEL1 – regulator of telomere elongation helicase 1
SDS-PAGE – sodium dodecyl sulfate polyacrylamide gel electrophoresis
TERRA – telomeric repeat-containing RNA
UTR – untranslated region
XPD – xeroderma pigmentosum group D
X-S – sulphur-containing intermediate

9 Literature

Reviews are marked with *

*Adam, Rodney D. 2021. "*Giardia duodenalis*: Biology and Pathogenesis." Clinical Microbiology Reviews 34 (4): e00024-19. https://doi.org/10.1128/CMR.00024-19.

*Baranovskiy, Andrey G., Hollie M. Siebler, Youri I. Pavlov, and Tahir H. Tahirov. 2018. "Iron–Sulfur Clusters in DNA Polymerases and Primases of Eukaryotes." Methods in Enzymology, vol. 599. Elsevier. https://doi.org/10.1016/bs.mie.2017.09.003.

*Barton, Jacqueline K., Rebekah M.B. Silva, and Elizabeth O'Brien. 2019. "Redox Chemistry in the Genome: Emergence of the [4Fe4S] Cofactor in Repair and Replication." Annual Review of Biochemistry 88 (1): 163–90. https://doi.org/10.1146/annurev-biochem-013118-110644.

Benga, W. J. 2005. "Distinct Regions of RPB11 Are Required for Heterodimerization with RPB3 in Human and Yeast RNA Polymerase II." Nucleic Acids Research 33 (11): 3582–90. https://doi.org/10.1093/nar/gki672.

Bertani, G. 1951. "STUDIES ON LYSOGENESIS I: The Mode of Phage Liberation by Lysogenic *Escherichia coli*." Journal of Bacteriology 62 (3): 293–300. https://doi.org/10.1128/jb.62.3.293-300.1951.

Boal, Amie K., Eylon Yavin, and Jacqueline K. Barton. 2007. "DNA Repair Glycosylases with a [4Fe–4S] Cluster: A Redox Cofactor for DNA-Mediated Charge Transport?" Journal of Inorganic Biochemistry 101 (11–12): 1913–21. https://doi.org/10.1016/j.jinorgbio.2007.05.001.

*Braymer, Joseph J., Sven A. Freibert, Magdalena Rakwalska-Bange, and Roland Lill. 2021. "Mechanistic Concepts of Iron-Sulfur Protein Biogenesis in Biology." Biochimica et Biophysica Acta (BBA) - Molecular Cell Research 1868 (1): 118863. https://doi.org/10.1016/j.bbamcr.2020.118863.

*Burgers, Peter M.J., and Thomas A. Kunkel. 2017. "Eukaryotic DNA Replication Fork." Annual Review of Biochemistry 86 (1): 417–38. https://doi.org/10.1146/annurev-biochem-061516-044709.

Buzuk, A, Md Marquez, Jv Ho, et al. 2025. "The Cia1 and Cia2 Subunits of the CTC Mediate Recognition of Apo-FeS Proteins with a C-Terminal Targeting Complex Recognition Motif." Preprint, Biochemistry, March 25. https://doi.org/10.1101/2025.03.25.645274.

Cavalier-Smith, Thomas. 2003. "Protist Phylogeny and the High-Level Classification of Protozoa." European Journal of Protistology 39 (4): 338–48. https://doi.org/10.1078/0932-4739-00002.

Cejka, Petr. 2015. “DNA End Resection: Nucleases Team Up with the Right Partners to Initiate Homologous Recombination.” Journal of Biological Chemistry 290 (38): 22931–38. https://doi.org/10.1074/jbc.R115.675942.

Chabrière, Eric, Marie-Helene Charon, Anne Volbeda, Laetitia Pieulle, Etienne Claude Hatchikian, and Juan-Carlos Fontecilla-Camps. 1999. Crystal Structures of the Key Anaerobic Enzyme Pyruvate:Ferredoxin Oxidoreductase, Free and in Complex with Pyruvate. https://doi.org/10.1038/5870.

Chanet, Roland, Dorothée Baïlle, Marie-Pierre Golinelli-Cohen, et al. 2021. “Fe-S Coordination Defects in the Replicative DNA Polymerase Delta Cause Deleterious DNA Replication in Vivo and Subsequent DNA Damage in the Yeast Saccharomyces Cerevisiae.” G3 Genes|Genomes|Genetics 11 (7): jkab124. https://doi.org/10.1093/g3journal/jkab124.

Chen, Huiqing, Jiayu Wei, Qi Tang, Guohui Li, Yajing Zhou, and Zhen Zhu. 2025. “Beyond Proofreading: POLD1 Mutations as Dynamic Orchestrators of Genomic Instability and Immune Evasion in Cancer.” Frontiers in Immunology 16 (June): 1600233. https://doi.org/10.3389/fimmu.2025.1600233.

Chepanoske, Cindy Lou, Marie-Pierre Golinelli, Scott D. Williams, and Sheila S. David. 2000. “Positively Charged Residues within the Iron–Sulfur Cluster Loop of *E. coli* MutY Participate in Damage Recognition and Removal.” Archives of Biochemistry and Biophysics 380 (1): 11–19. https://doi.org/10.1006/abbi.2000.1890.

Collins, Brett M., Airlie J. McCoy, Helen M. Kent, Philip R. Evans, and David J. Owen. 2002. “Molecular Architecture and Functional Model of the Endocytic AP2 Complex.” Cell 109 (4): 523–35. https://doi.org/10.1016/S0092-8674(02)00735-3.

Constantinescu-Aruxandei, Diana, Biljana Petrovic-Stojanovska, J. Carlos Penedo, Malcolm F. White, and James H. Naismith. 2016. “Mechanism of DNA Loading by the DNA Repair Helicase XPD.” Nucleic Acids Research 44 (6): 2806–15. https://doi.org/10.1093/nar/gkw102.

Crack, Jason C., Jeffrey Green, Andrew J. Thomson, and Nick E. Le Brun. 2014. “Iron–Sulfur Clusters as Biological Sensors: The Chemistry of Reactions with Molecular Oxygen and Nitric Oxide.” Accounts of Chemical Research 47 (10): 3196–205. https://doi.org/10.1021/ar5002507.

Cunningham, Richard P, Hitomi Asahara, Janet F Bank, et al. 1989. Endonuclease III Is an Iron-Sulfur Proteid. Nature structural biology, 6(2), 182-190.

*Datta, Arindam, and Robert M. Brosh. 2018. “New Insights Into DNA Helicases as Druggable Targets for Cancer Therapy.” Frontiers in Molecular Biosciences 5 (June): 59. https://doi.org/10.3389/fmolb.2018.00059.

De Rosa, Mariarosaria, Ryan P. Barnes, Ariana C. Detwiler, Prasanth R. Nyalapatla, Peter Wipf, and Patricia L. Opresko. 2025. “OGG1 and MUTYH Repair Activities Promote Telomeric 8-Oxoguanine Induced Senescence in Human Fibroblasts.” Nature Communications 16 (1): 893. https://doi.org/10.1038/s41467-024-55638-4.

Di Matteo, Adele, Francesca Maria Scandurra, Fabrizio Testa, et al. 2008. “The O2-Scavenging Flavodiiron Protein in the Human Parasite *Giardia intestinalis*.” Journal of Biological Chemistry 283 (7): 4061–68. https://doi.org/10.1074/jbc.M705605200.

Duwor, Seth, Daniela Brites, and Pascal Mäser. 2024. “Phylogenetic Analysis of Pyruvate-Ferredoxin Oxidoreductase, a Redox Enzyme Involved in the Activation of Nitro-Based Prodrugs in Bacteria and Protozoa.” Preprint, Biology and Life Sciences, March 1. https://doi.org/10.20944/preprints202311.1649.v2.

Emelyanov, Victor V., and Alina V. Goldberg. 2011. “Fermentation Enzymes of *Giardia intestinalis*, Pyruvate:Ferredoxin Oxidoreductase and Hydrogenase, Do Not Localize to Its Mitosomes.” Microbiology 157 (6): 1602–11. https://doi.org/10.1099/mic.0.044784-0.

Faso, Carmen, and Adrian B. Hehl. 2011. “Membrane Trafficking and Organelle Biogenesis in *Giardia lamblia*: Use It or Lose It.” International Journal for Parasitology 41 (5): 471–80. https://doi.org/10.1016/j.ijpara.2010.12.014.

Frey, Avery G., Daniel J. Palenchar, Justin D. Wildemann, and Caroline C. Philpott. 2016. “A Glutaredoxin·BolA Complex Serves as an Iron-Sulfur Cluster Chaperone for the Cytosolic Cluster Assembly Machinery.” Journal of Biological Chemistry 291 (43): 22344–56. https://doi.org/10.1074/jbc.M116.744946.

Gerber, Jana, Karina Neumann, Corinna Prohl, Ulrich Mühlenhoff, and Roland Lill. 2004. “The Yeast Scaffold Proteins Isu1p and Isu2p Are Required inside Mitochondria for Maturation of Cytosolic Fe/S Proteins.” Molecular and Cellular Biology 24 (11): 4848–57. https://doi.org/10.1128/MCB.24.11.4848-4857.2004.

Ghisays, Fiorella, Aitor Garzia, Hexiao Wang, et al. 2021. “RTEL1 Influences the Abundance and Localization of TERRA RNA.” Nature Communications 12 (1): 3016. https://doi.org/10.1038/s41467-021-23299-2.

*Gillet, Ludovic C. J., and Orlando D. Schärer. 2006. “Molecular Mechanisms of Mammalian Global Genome Nucleotide Excision Repair.” Chemical Reviews 106 (2): 253–76. https://doi.org/10.1021/cr040483f.

Gutiérrez, Lester, Nadja A. Vielot, Roberto Herrera, et al. 2024. “*Giardia lamblia* Risk Factors and Burden in Children with Acute Gastroenteritis in a Nicaraguan Birth Cohort.” PLOS Neglected Tropical Diseases 18 (11): e0012230. https://doi.org/10.1371/journal.pntd.0012230.

Hanahan, Douglas. 1983. “Studies on Transformation of *Escherichia coli* with Plasmids.” Journal of Molecular Biology 166 (4): 557–80. https://doi.org/10.1016/S0022-2836(83)80284-8.

Hassan, Ayaz, Filipe C. D. A. Lima, and Frank N. Crespilho. 2025. “Redox-Guided DNA Scanning by the Dynamic Repair Enzyme Endonuclease III.” Biochemistry 64 (4): 782–90. https://doi.org/10.1021/acs.biochem.4c00621.

Iyer, L. M. 2005. “Origin and Evolution of the Archaeo-Eukaryotic Primase Superfamily and Related Palm-Domain Proteins: Structural Insights and New Members.” Nucleic Acids Research 33 (12): 3875–96. https://doi.org/10.1093/nar/gki702.

Jain, Rinku, Eva S. Vanamee, Boris G. Dzikovski, et al. 2014. “An Iron–Sulfur Cluster in the Polymerase Domain of Yeast DNA Polymerase ε.” Journal of Molecular Biology 426 (2): 301–8. https://doi.org/10.1016/j.jmb.2013.10.015.

Jedelský, Petr L., Pavel Doležal, Petr Rada, et al. 2011. “The Minimal Proteome in the Reduced Mitochondrion of the Parasitic Protist *Giardia intestinalis*.” PLoS ONE 6 (2): e17285. https://doi.org/10.1371/journal.pone.0017285.

*Johnson, Michael K. 1998. “Iron—Sulfur Proteins: New Roles for Old Clusters.” Current Opinion in Chemical Biology 2 (2): 173–81. https://doi.org/10.1016/S1367-5931(98)80058-6.

Jozwiakowski, Stanislaw K., Sandra Kummer, and Kerstin Gari. 2019. “Human DNA Polymerase Delta Requires an Iron–Sulfur Cluster for High-Fidelity DNA Synthesis.” Life Science Alliance 2 (4): e201900321. https://doi.org/10.26508/lsa.201900321.

Kassube, Susanne A., and Nicolas H. Thomä. 2020. “Structural Insights into Fe–S Protein Biogenesis by the CIA Targeting Complex.” Nature Structural & Molecular Biology 27 (8): 735–42. https://doi.org/10.1038/s41594-020-0454-0.

Keister, David B. 1983. “Axenic Culture of Giardia Lamblia in TYI-S-33 Medium Supplemented with Bile.” Transactions of the Royal Society of Tropical Medicine and Hygiene 77 (4): 487–88. https://doi.org/10.1016/0035-9203(83)90120-7.

Kunkel, Thomas A, and Peter M Burgers. 2014. “Delivering Nonidentical Twins.” Nature Structural & Molecular Biology 21 (8): 649–51. https://doi.org/10.1038/nsmb.2852.

Kuper, Jochen, Cathy Braun, Agnes Elias, et al. 2014. “In TFIIH, XPD Helicase Is Exclusively Devoted to DNA Repair.” PLoS Biology 12 (9): e1001954. https://doi.org/10.1371/journal.pbio.1001954.

Landry, Aaron P., and Huangen Ding. 2014. “The N-Terminal Domain of Human DNA Helicase Rtel1 Contains a Redox Active Iron-Sulfur Cluster.” BioMed Research International 2014: 1–8. https://doi.org/10.1155/2014/285791.

Li, Ping, Amber L. Hendricks, Yong Wang, et al. 2022. “Structures of Atm1 Provide Insight into [2Fe-2S] Cluster Export from Mitochondria.” Nature Communications 13 (1): 4339. https://doi.org/10.1038/s41467-022-32006-8.

*Lill, Roland. 2009. “Function and Biogenesis of Iron–Sulphur Proteins.” Nature 460 (7257): 831–38. https://doi.org/10.1038/nature08301.

Lisova Alisa E., Andrey G. Baranovskiy, Lucia M. Morstadt, Nigar D. Babayeva, Elena I. Stepchenkova, and Tahir H. Tahirov. 2022. “The Iron-Sulfur Cluster Is Critical for DNA Binding by Human DNA Polymerase ε.” Preprint, Biochemistry, May 5. https://doi.org/10.1101/2022.05.05.490830.

Liu, Huanting, Jana Rudolf, Kenneth A. Johnson, et al. 2008. “Structure of the DNA Repair Helicase XPD.” Cell 133 (5): 801–12. https://doi.org/10.1016/j.cell.2008.04.029.

McInally, S. G., K. D. Hagen, C. Nosala, et al. 2019. “Robust and Stable Transcriptional Repression in Giardia Using CRISPRi.” Molecular Biology of the Cell 30 (1): 119–30. https://doi.org/10.1091/mbc.E18-09-0605.

*Mendel, Ralf R., Thomas W. Hercher, Arkadiusz Zupok, Muhammad A. Hasnat, and Silke Leimkühler. 2020. "The Requirement of Inorganic Fe-S Clusters for the Biosynthesis of the Organometallic Molybdenum Cofactor" *Inorganics* 8, no. 7: 43. https://doi.org/10.3390/inorganics8070043.

Moiseeva, Tatiana N., Armin M. Gamper, Brian L. Hood, Thomas P. Conrads, and Christopher J. Bakkenist. 2016. “Human DNA Polymerase ε Is Phosphorylated at Serine-1940 after DNA Damage and Interacts with the Iron-Sulfur Complex Chaperones CIAO1 and MMS19.” DNA Repair 43 (July): 9–17. https://doi.org/10.1016/j.dnarep.2016.04.007.

Motyčková, Alžběta, Luboš Voleman, Vladimíra Najdrová, et al. 2023. “Adaptation of the Late ISC Pathway in the Anaerobic Mitochondrial Organelles of *Giardia intestinalis*.” PLOS Pathogens 19 (10): e1010773. https://doi.org/10.1371/journal.ppat.1010773.

Netz, Daili J A, Antonio J Pierik, Martin Stümpfig, Ulrich Mühlenhoff, and Roland Lill. 2007. “The Cfd1–Nbp35 Complex Acts as a Scaffold for Iron-Sulfur Protein Assembly in the Yeast Cytosol.” Nature Chemical Biology 3 (5): 278–86. https://doi.org/10.1038/nchembio872.

Netz, Daili J A, Carrie M Stith, Martin Stümpfig, et al. 2012. “Eukaryotic DNA Polymerases Require an Iron-Sulfur Cluster for the Formation of Active Complexes.” Nature Chemical Biology 8 (1): 125–32. https://doi.org/10.1038/nchembio.721.

Netz, Daili J A, Martin Stümpfig, Carole Doré, Ulrich Mühlenhoff, Antonio J Pierik, and Roland Lill. 2010. “Tah18 Transfers Electrons to Dre2 in Cytosolic Iron-Sulfur Protein Biogenesis.” Nature Chemical Biology 6 (10): 758–65. https://doi.org/10.1038/nchembio.432.

O’Brien, Elizabeth, Marilyn E. Holt, Matthew K. Thompson, et al. 2017. “The [4Fe-4S] Cluster of Human DNA Primase Functions as a Redox Switch Using DNA Charge Transport.” Science 355 (6327): eaag1789. https://doi.org/10.1126/science.aag1789.

Pandey, Ashutosh K., Jayashree Pain, Andrew Dancis, and Debkumar Pain. 2019. “Mitochondria Export Iron–Sulfur and Sulfur Intermediates to the Cytoplasm for Iron–Sulfur Cluster Assembly and tRNA Thiolation in Yeast.” Journal of Biological Chemistry 294 (24): 9489–502. https://doi.org/10.1074/jbc.RA119.008600.

Peng, Guang, Hui Dai, Wei Zhang, et al. 2012. “Human Nuclease/Helicase DNA2 Alleviates Replication Stress by Promoting DNA End Resection.” Cancer Research 72 (11): 2802–13. https://doi.org/10.1158/0008-5472.CAN-11-3152.

Pokharel, Subhash, and Judith L. Campbell. 2012. “Cross Talk between the Nuclease and Helicase Activities of Dna2: Role of an Essential Iron–Sulfur Cluster Domain.” Nucleic Acids Research 40 (16): 7821–30. https://doi.org/10.1093/nar/gks534.

Pyrih, Jan, Eva Pyrihová, Martin Kolísko, et al. 2016. “Minimal Cytosolic Iron-sulfur Cluster Assembly Machinery of *Giardia intestinalis* Is Partially Associated with Mitosomes.” Molecular Microbiology 102 (4): 701–14. https://doi.org/10.1111/mmi.13487.

Pyrih, Jan, Vojtěch Žárský, Justin D. Fellows, et al. 2021. “The Iron-Sulfur Scaffold Protein HCF101 Unveils the Complexity of Organellar Evolution in SAR, Haptista and Cryptista.” BMC Ecology and Evolution 21 (1): 46. https://doi.org/10.1186/s12862-021-01777-x.

Rafferty, Steven, Betty Luu, Raymond E. March, and Janet Yee. 2010. “*Giardia lamblia* Encodes a Functional Flavohemoglobin.” Biochemical and Biophysical Research Communications 399 (3): 347–51. https://doi.org/10.1016/j.bbrc.2010.07.073.

Rudolf, Jana, Vasso Makrantoni, W. John Ingledew, Michael J.R. Stark, and Malcolm F. White. 2006. “The DNA Repair Helicases XPD and FancJ Have Essential Iron-Sulfur Domains.” Molecular Cell 23 (6): 801–8. https://doi.org/10.1016/j.molcel.2006.07.019.

Schindelin, Johannes, Ignacio Arganda-Carreras, Erwin Frise, et al. 2012. “Fiji: An Open-Source Platform for Biological-Image Analysis.” Nature Methods 9 (7): 676–82. https://doi.org/10.1038/nmeth.2019.

Shin, Yeonoh, Mark Hedglin, and Katsuhiko S. Murakami. 2025. “Cryo-EM Structure of Apo-Form Human DNA Polymerase δ Elucidates Its Minimal DNA Synthesis Activity without PCNA.” Journal of Biological Chemistry 301 (4): 108342. https://doi.org/10.1016/j.jbc.2025.108342.

Smith, Duncan J., and Iestyn Whitehouse. 2012. “Intrinsic Coupling of Lagging-Strand Synthesis to Chromatin Assembly.” Nature 483 (7390): 434–38. https://doi.org/10.1038/nature10895.

Sontz, Pamela A., Timothy P. Mui, Jill O. Fuss, John A. Tainer, and Jacqueline K. Barton. 2012. “DNA Charge Transport as a First Step in Coordinating the Detection of Lesions by Repair Proteins.” Proceedings of the National Academy of Sciences 109 (6): 1856–61. https://doi.org/10.1073/pnas.1120063109.

Soultanas, Panos, Mark S. Dillingham, Paul Wiley, Martin R. Webb, and Dale B. Wigley. 2000. “Uncoupling DNA Translocation and Helicase Activity in PcrA: Direct Evidence for an Active Mechanism.” The EMBO Journal 19 (14): 3799–810. https://doi.org/10.1093/emboj/19.14.3799.

Sviderskiy, Vladislav O., Lili Blumenberg, Elizabeth Gorodetsky, et al. 2020. “Hyperactive CDK2 Activity in Basal-like Breast Cancer Imposes a Genome Integrity Liability That Can Be Exploited by Targeting DNA Polymerase ε.” Molecular Cell 80 (4): 682-698.e7. https://doi.org/10.1016/j.molcel.2020.10.016.

ter Beek, Josy, Vimal Parkash, Göran O Bylund, Pia Osterman, A Elisabeth Sauer-Eriksson, and Erik Johansson. 2019. “Structural Evidence for an Essential Fe–S Cluster in the Catalytic Core Domain of DNA Polymerase ϵ.” Nucleic Acids Research 47 (11): 5712–22. https://doi.org/10.1093/nar/gkz248.

Tovar, Jorge, Gloria León-Avila, Lidya B Sánchez, et al. 2003. “Mitochondrial Remnant Organelles of *Giardia* Function in Iron-Sulphur Protein Maturation.” Nature 426 (6963): 172–76. https://doi.org/10.1038/nature01945.

Townson, Steven M., Jacqueline A. Upcroft, and Peter Upcroft. 1996. “Characterisation and Purification of Pyruvate:Ferredoxin Oxidoreductase from *Giardia duodenalis*.” Molecular and Biochemical Parasitology 79 (2): 183–93. https://doi.org/10.1016/0166-6851(96)02661-8.

*Tsaousis, Anastasios D. 2019. “On the Origin of Iron/Sulfur Cluster Biosynthesis in Eukaryotes.” Frontiers in Microbiology 10 (November): 2478. https://doi.org/10.3389/fmicb.2019.02478.

Tse, Edmund C. M., Theodore J. Zwang, Sebastian Bedoya, and Jacqueline K. Barton. 2019. “Effective Distance for DNA-Mediated Charge Transport between Repair Proteins.” ACS Central Science 5 (1): 65–72. https://doi.org/10.1021/acscentsci.8b00566.

Urzica, Eugen, Antonio J. Pierik, Ulrich Mühlenhoff, and Roland Lill. 2009. “Crucial Role of Conserved Cysteine Residues in the Assembly of Two Iron−Sulfur Clusters on the CIA Protein Nar1.” Biochemistry 48 (22): 4946–58. https://doi.org/10.1021/bi900312x.

*White, Malcolm F. 2009. “Structure, Function and Evolution of the XPD Family of Iron–Sulfur-Containing 5′→3′ DNA Helicases.” Biochemical Society Transactions 37 (3): 547–51. https://doi.org/10.1042/BST0370547.

*Wu, Y., and R. M. Brosh. 2012. “DNA Helicase and Helicase-Nuclease Enzymes with a Conserved Iron-Sulfur Cluster.” Nucleic Acids Research 40 (10): 4247–60. https://doi.org/10.1093/nar/gks039.

Wu, Y., A. N. Suhasini, and R. M. Brosh. 2009. “Welcome the Family of FANCJ-like Helicases to the Block of Genome Stability Maintenance Proteins.” Cellular and Molecular Life Sciences 66 (7): 1209–22. https://doi.org/10.1007/s00018-008-8580-6.

Yuan, Zuanning, Roxana Georgescu, Grant D. Schauer, Michael E. O’Donnell, and Huilin Li. 2020. “Structure of the Polymerase ε Holoenzyme and Atomic Model of the Leading Strand Replisome.” Nature Communications 11 (1): 3156. https://doi.org/10.1038/s41467-020-16910-5.

Zachayus, Amélie, Jules Loup-Forest, Vincent Cura, and Arnaud Poterszman. 2025. “Nucleotide Excision Repair: Insights into Canonical and Emerging Functions of the Transcription/DNA Repair Factor TFIIH.” Genes 16 (2): 231. https://doi.org/10.3390/genes16020231.

Zerbe, Laura K., and Robert D. Kuchta. 2002. “The P58 Subunit of Human DNA Primase Is Important for Primer Initiation, Elongation, and Counting.” Biochemistry 41 (15): 4891–900. https://doi.org/10.1021/bi016030b.

Zhang, Yinbo, Andrey G. Baranovskiy, Tahir H. Tahirov, and Youri I. Pavlov. 2014. “The C-Terminal Domain of the DNA Polymerase Catalytic Subunit Regulates the Primase and Polymerase Activities of the Human DNA Polymerase α-Primase Complex.” Journal of Biological Chemistry 289 (32): 22021–34. https://doi.org/10.1074/jbc.M114.570333.

Zhou, Chun, Sergei Pourmal, and Nikola P Pavletich. 2015. “Dna2 Nuclease-Helicase Structure, Mechanism and Regulation by Rpa.” eLife 4 (November): e09832. https://doi.org/10.7554/eLife.09832.